Structural and structure-function correlations in neurodevelopmental and aging disorders of the visual system

Frederico Ramiro Santos Lourenço

P.I.: Professor Miguel Castelo-Branco, M.D., Ph.D.

Visual Neuroscience Laboratory, IBILI, University of Coimbra, Portugal

Integrated Master's Project in Biomedical Engineering, University of Coimbra

July 2010

Acknowledgments

Este trabalho só foi possível graças à excelente equipa de investigação em neurociências do IBILI. Em particular gostaria de agradecer ao meu orientador, Professor Miguel Castelo-Branco, pela discussão de ideias, conselhos e apoio desde a minha chegada ao grupo de trabalho. Obrigado ao Gil Cunha e à Inês Violante pelos ensinamentos sobre o BrainVoyager (mais valiosos que qualquer tutorial), à Mafalda Martins e Bárbara Oliveiros pelo trabalho incansável na análise estatística, à Catarina Mateus pelo recrutamento dos pacientes e por todos os dados oftalmológicos fornecidos, e ao Carlos Ferreira e João Marques pela ajuda permanente na aquisição dos dados fMRI. A todos, muito obrigado.

Contents

1. Introduction
   - 1.1. Neurobiology of the visual system
   - 1.2. Retinotopic mapping
   - 1.3. Objectives

2. Methods to study structure and function of visual pathways
   - 2.1. Cortical Thickness Analysis (CTA)
   - 2.2. Methods in Retinotopy
   - 2.3. Retinal and RNFL thickness measurements
   - 2.4. Methods to study visual function in retinocortical disease

3. Results: Structural and structure-function correlations
   - 3.1. Glaucoma (1st part of the study)
     - 3.1.1. Cortical thickness of retinotopic areas
     - 3.1.2. Correlations between thickness of retinotopic areas and the retinal nerve fiber layer of the optic nerve (RNFL)
     - 3.1.3. Correlations between thickness of retinotopic areas and sensory function (as measured by the FDT – frequency doubling contrast sensitivity technique)
     - 3.1.4. Multivariate analysis of variance (MANOVA) and CatPCA (Principal Component Analysis
   - 3.2. Leber Hereditary Optic Neuropathy (2nd part of the study)
     - 3.2.1. Cortical thickness of retinotopic areas
     - 3.2.2. Correlations between thickness of retinotopic areas and retinal nerve fiber layer of the optic nerve (RNFL) and of the macula at distinct eccentricities
     - 3.2.3. Correlations between thickness of retinotopic areas and sensory function as measured by standard perimetry (SAP)
     - 3.2.4. CatPCA and FA (factor analysis)

4. Discussion
5. References

Abbreviations

OE – left eye

OD – right eye

VF – visual field

CT – cortical thickness

RNFL – retinal nerve fiber layer

LH – left hemifield (VF) or left hemisphere (cortex)

RH – right hemifield (VF) or right hemisphere (cortex)

WM – White matter

GM – Grey matter

CSF – Cerebrospinal fluid

TS – Temporal/Superior quadrant (VF)

NS – Nasal/Superior quadrant (VF)

TI – Temporal/Inferior quadrant (VF)

NI – Nasal/Inferior (VF)

V1 – primary visual cortex

V2d – dorsal V2 (extrastriate visual area)

V2v – ventral V2 (extrastriate visual area)

V3 – dorsal V3 (extrastriate visual area)

VP – ventral V3 (extrastriate visual area)

OCT – Optical coherence tomography

SAP – Standard automated perimetry

FA – Factor Analysis

CatPCA – Principal Component Analysis for categorical data

Chapter 1

Introduction

Neurobiology of the visual system

The visual system is part of the central nervous system (CNS) and underlies our ability to see. Vision is one of the senses we use to gather information about the surrounding environment. The light that reflects or irradiates from the environment enters the eye and is projected onto the retina. In its deepest layer, photoreceptors convert the patterns of light into electrical signals that neurons convey to the visual cortex. In a simplistic way, this system captures visible light and interprets its information in order to create a representation of the external world.

However, the biology behind vision is far from being simple. Our eyes and brain work together to accomplish a multitude of complex tasks: since the light enters our eyes till we experience the psychological manifestation of that visual information (i.e., till we 'see'), a number of structures, connecting pathways and brain regions are recruited to process and relay the relevant signals. For instance, to retrieve detailed visual information from an object, it must be projected on the fovea – this is the area of the retina with the highest concentration of photoreceptors – in order to provide the highest visual acuity. Therefore, to keep the (moving) object's projection on the fovea, brain and eyes interact through reflex and voluntary eyes movements (e.g., slow, smooth pursuit eye movements and fast, saccadic eye movements).

Eye

The eyes are organs that evolved to detect light, convert it to electrical impulses and relay those signals along the optic nerve towards the visual cortex, in the brain. These organs vary tremendously in shape (generally divided into ten different forms) and functional organization; nevertheless, 96% of all animal species possess a complex optical system. (Land et al., 1992). Some of the basic surrounding characteristics captured by the eyes are shape, color and movement. But vision is a highly specialized sense that evolved to suit particular needs. For example, predators

of the eye structure

ates.

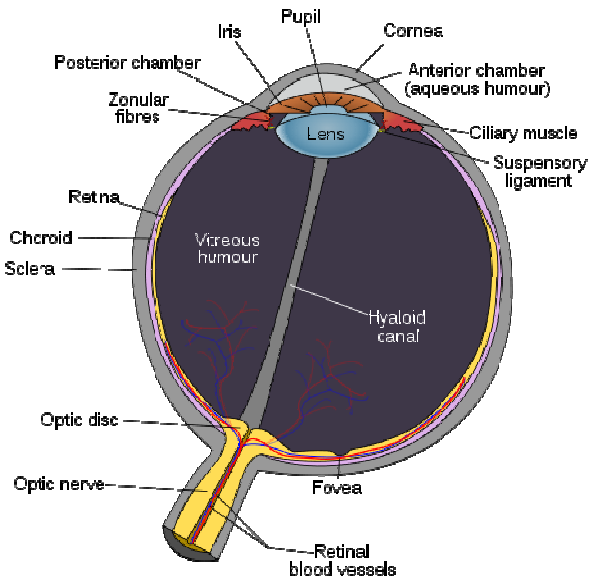

(e.g., humans) have both eyes aiming forward; this provides large areas of binocular vision which is ideal for target localization and stereoscopic depth perception. On the other hand, animals that require a broader coverage of the visual field – to avoid being preyed upon – have their eyes pointing sideways (monocular vision).

Retina

The retina is a thin, filmy tissue, less than half millimeter thick, that covers the internal part of the eye. It consists of a stack of cellular layers, each with a specific role. There are three layers of nerve cells separated by two layers of synaptic connections. The first layer starting from the back of the eye (the furthest from the light source) is made of a large number of photoreceptor cells, which are sensitive to light. There are two main types of cells, rods and cones, with distinct functions: the first are very sensitive to light – ideal for low light conditions – and can be found in high numbers throughout the retina, while the latter are much less sensitive to light, but provide color perception (although much sparser than rods, cones are highly concentrated on the fovea). Cones can be subdivided into three types, according to the wavelengths of light they preferentially absorb: therefore, they are known as *blue*, *green* and *red* cones.

The unique trait of these retinian cells is the fact they contain special proteins – opsins – that have the ability to absorb photons. Such absorption triggers a signal transduction pathway, which starts with the conformational change of *retinal* (vitamin A) and eventually hyperpolarizes the photoreceptor cells, giving rise to an electrical signal. Once retinal molecules undergo this process, they are taken by the pigment epithelium – the tissue behind the retina that is usually dark due to its melanin content – to be recycled. This pigment plays an important role by absorbing photons after they cross the photoreceptive layer, which prevents their reflection and deterioration of overall image quality (Kolb, 2003).

Subsequently, the neuronal impulses are transmitted to the following layer, mainly composed of bipolar cells. These cells can synapse with either cones or rods and may also receive input from horizontal cells. Bipolar cells can be either of *ON* or *OFF* type, depending on their reaction to glutamate released by photoreceptor cells (such release is inversely related to the amount of light that photoreceptors capture). Intuitively, when light is detected, glutamate concentration decreases and *ON* bipolar cells depolarize; on the other hand, *OFF* bipolar cells will react in the opposite way, by hyperpolarizing. Under low light conditions, however, photoreceptor cells release more glutamate, which then inhibits the ON cells and excites the OFF bipolar cells (Nicholls et al., 2001). Subsequently, the bipolar cells transmit signals to the third, outermost

layer, which consists of retinal ganglion cells (RGC's); these will finally output action potentials to the brain.

The RGC's, although presenting diversified characteristics, have the common property of extending a long axon into the brain. This may explain why they fire action potentials, unlike photoreceptors and bipolar cells. These axons exit the retina in bundles and form the optic nerve (which then extends towards the optic chiasm and the optic tract). Although a small part of the ganglion cells is not dedicated to vision (e.g., RGC's involved in the circadian rhythm and pupillary light reflex), most of the 1.2 – 1.5 million of cells present in the human retina are engaged in visual processing, transmitting visual information from the retina to the thalamus, hypothalamus and midbrain. This mechanism depends on the modulation of the ganglion cells: when stimuli are not present (resting state), RGC's fire at a baseline rate; upon excitation of the central part of the receptive field of stimuli of appropriate polarity (black/white depending on whether the cell belongs to the OFF or ON pathway), they increase the firing rate, while inhibition of the cells by stimulus placement on surrounding regions reduces it.

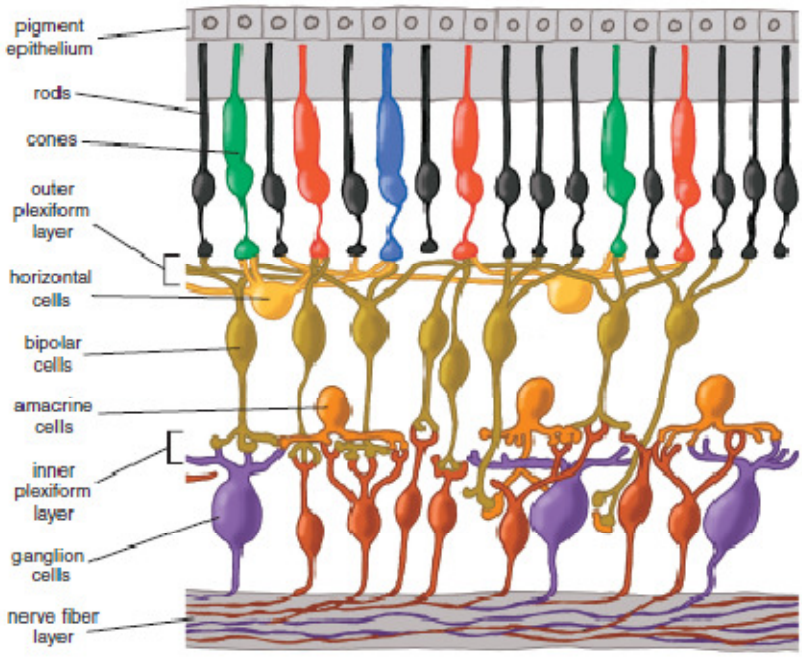

Fig. 2: Representation of the discrete layers of retinal cells; light travels upwards crossing the nerve fiber layer first and finally reaching the pigment epithelium. It is noteworthy the presence of neurons in the retina, particularly horizontal and amacrine cells, which can relay information laterally (between neurons of the same layer); these cells are known to integrate and regulate information transfer in inner and outer plexiform layers (Kolb, 2003).

An interesting aspect of the human retina is its peculiar architecture as, theoretically, one might expect to encounter the photoreceptor cells on the inner layer, in order to optimize the photon capture when they enter the eye. However, evolution has led to a different design, where light has to cross multiple layers of nerve cells and synaptic fibers until it reaches the photo-sensitive cells.

In conclusion, the retina is a complex tissue that consists of both sensory (photo-sensitive) neurons that interact with light and neural circuits that are responsible for the initial image processing; this information is then passed on through the optic nerve into the brain to eventually form a visual perception of the outside world, which is the phenomenon we consciously interpret as *seeing*.

Receptive fields

In the visual system, sensory neurons can be stimulated (i.e., their firing rate increases) by the presence of a (light) stimulus coming from a particular region of space – known as a receptive field. Particularly, for a photoreceptor, this region corresponds to a volume in space (with a conic shape) from where light can converge and excite the cell. However, visual receptive fields are commonly illustrated in two dimensions, which represents a cut along the volume of space which a specific cell responds to. Not surprisingly, the level of complexity rises when we broaden the concept of receptive fields, extending them to a more intricate neural system (they have been mapped all the way to the lateral geniculate nucleus and visual cortex cells). This leads to the notion of center surround organization, whereby an appropriate stimulus placed in the center will activate the cell, whereas when it is placed in the surround it inhibits the same neuron. This type of organization starts already at the bipolar cell level. Neighboring photoreceptors

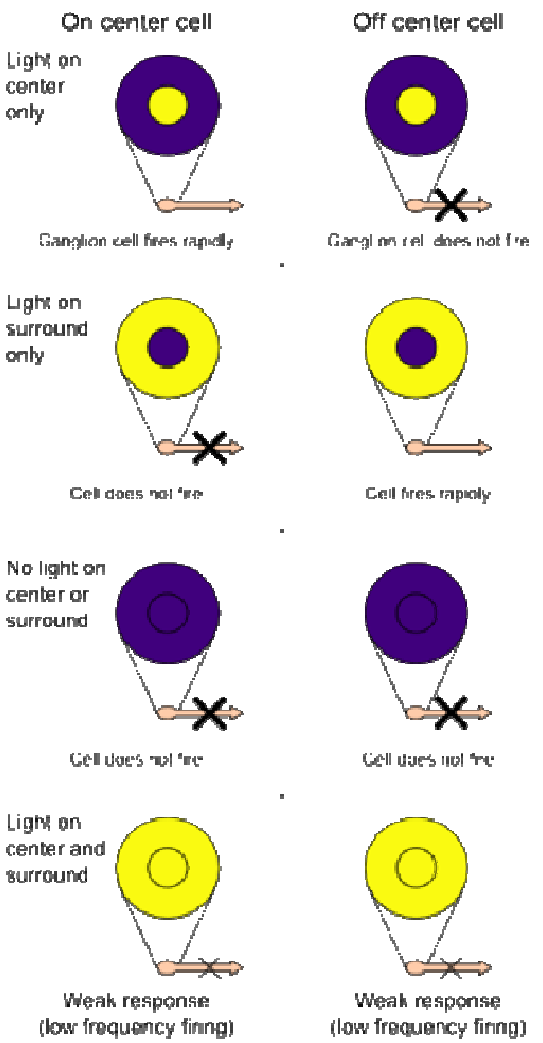

lds and cell firing.

are known to communicate (i.e., to form synapses) with a single cell (e.g., bipolar cell); therefore, the receptive field of the latter is nothing less than the combined fields of the cells that are providing it with visual input. In fact, the formation of center-surround receptive fields of bipolar and ganglion cells accounts for a significant amount of the visual processing that already takes place in the retina.

In the same line of thought, the receptive field of a RGC encompasses the input from all photoreceptors that are linked (through bipolar, horizontal and amacrine cells) to it and, finally, a cell in the brain has an even larger receptive field as it synapses with a group of ganglion cells. This process is known as *convergence* and was first described by Hubel and Wiesel; in a pioneering study performed in the cat visual system, they have claimed that receptive fields of cells at an higher level of the visual system arise from input received by cells at a lower level. In this way, smaller fields from a group of receptors 'funnel into a particular ganglion cell…and that group forms the ganglion cell's receptive field'. (Hubel et al., 1963). Later on, this hierarchical organization has increased in complexity by allowing cells to receive feedback from higher levels of the visual system.

From the eye to the brain

The visual pathway between the retina and the brain consists of an optic nerve, the optic chiasma (where the nerves partially cross) and is primarily made of axons from ganglion cells. The vast majority of these axons belong to M and P ganglion cells and extend towards the lateral geniculate nucleus (LGN) in the thalamus; this parallel networks of ganglion cells will allow the visual cortex to analyze aspects of the visual word beyond contrast or luminance (e.g., form, color and movement).

- P (*Parvo*) cells have small center-surround receptive fields with slow conduction speed; their axons are projected into the parvocellular layers of the LGN; these cells exist in higher number than any other RGC type and in central retina, where cone density is maximum, there are two P cells for each cone (Gazzaniga, 2004). P cells provide superb visual acuity and play a major role in color vision (they respond selectively to specific chromatic contrasts given the specific organization of cone input to center and surround mechanisms).
- M (Magno) cells have much larger center-surround receptive fields, fast conduction speed and large dendritic trees (receiving input from many photoreceptors); their axons are projected into the magnocellular layers of the LGN. M cells account for less than 10% of RGC's and are particularly sensitive to achromatic stimuli, even in low-contrast conditions; they appear to have a role in the perception of gross features and movement (Kandel et al., 2000).

- K (Konio) cells project their axons into the koniocellular layers of the LGN; they are very small and 'have a density of approximately 1% of the total ganglion cells in central retina, increasing to approximately 6-10% in the retinal periphery' (Dacey, 1993). K cells have very large receptive fields, most of them with blue-ON center and blue-OFF (yellow) surround. This means that ON center receives input from blue cones and the OFF center receives input from red and green cones; they are thought to provide an additional function in color vision.

Lateral Geniculate Nucleus (LGN)

The LGN is a major processing center of visual information and is located in the thalamus (there is one LGN in each brain hemisphere). As previously referred to, it receives such information from the retinal ganglions cells through the optic tract; on the other hand, output relay-neurons of the LGN send axons through a pathway – the optic radiation – that leads to the primary visual cortex, or V1 (this, in turn, sends feedback connections back to the LGN through its layer 6).

The human LGN has a peculiar organization of six layers, with two subdivisions of four dorsal, parvocellular layers and two ventral, magnocellular layers. But differences go beyond their distinct anatomy; functionally, these subdivisions represent different facets of vision. In 1920, Minkowski discovered the projection tracts between the retina and the thalamus and proved that homonymous areas of the retina (i.e., the visual information, captured from both eyes, coming from a specific region of the visual field) are aligned together in the projection field of the LGN; these findings had a tremendous impact on cortical processing depth perception, or three-dimensional binocular vision as they provide the possibility for the combination of binocular information at higher levels (Minkowski, 1920). Interestingly, each eye projects to three layers of each lateral geniculate body, in an alternating way. Therefore, a visual hemifield (corresponds to half of the retina) is represented three times in each LGN, twice on parvocellular layers and once on the magnocellular layer. It is important to recall that the former layers are known to be particularly involved in form and color perception, while the latter is responsible for movement and gross depth perception. (Livingstone et al., 1988).

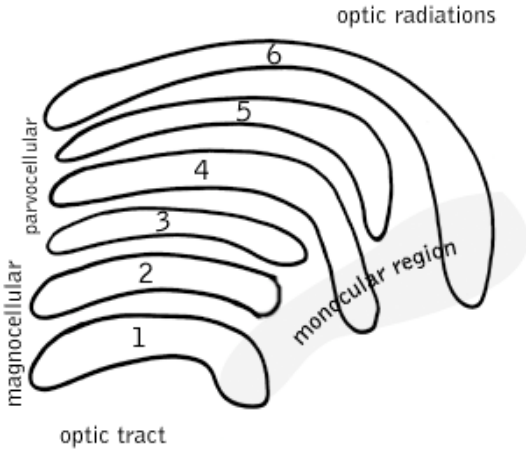

Fig. 4: Schematic structure of the LGN; the inner layers, 1 and 2, are the magnocellular, while the outer four are the parvocellular layers.

In between these layers, there are K cells which provide a third route to the visual cortex. So far, the functional role of the koniocellular system, despite being functionally different from either M and P cells, is still unclear.

Although overall LGN function in visual perception remains unclear, it has been proposed that after receiving the spatially decorrelated visual information from the retina, the LGN performs temporal decorrelation to bring the visual data one step closer to the visual processing that will take place at the cortical level. (Dong et al., 1995).

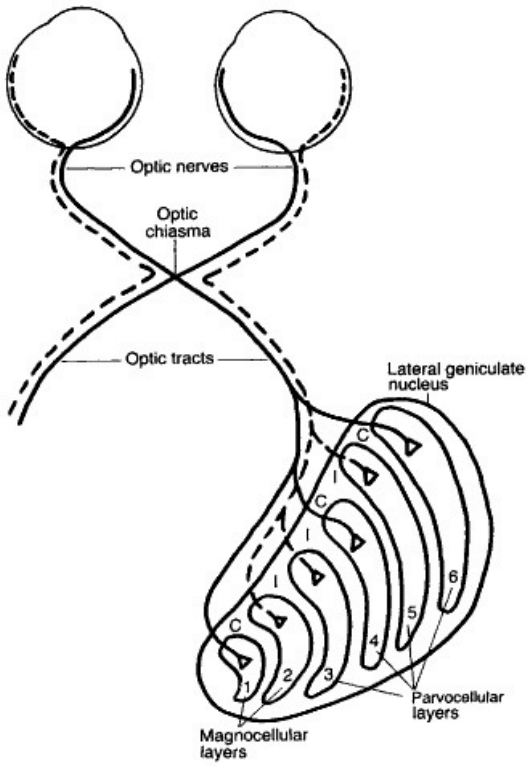

Fig. 5: Optic fibers from the nasal halves of the retina cross at the optic chiasm. Within the LGN, the visual information coming from the *contralateral* eye is transferred to layers 1,4 and 6; the visual information from the *ipsilateral* eye, in an alternating fashion, is passed to layers 2,3 and 5 (Wade et al., 1991).

Visual decussation

The lateral geniculate body on each hemisphere receives visual input from both eyes. To achieve this anatomically, our visual system has evolved in a way that allows part of the optic nerve fibers to decussate. The axons of the ganglion cells from the inner (nasal) side of the retina cross to the opposite (or *contralateral*) hemisphere through the optic chiasm, while those from the outer (temporal) side of the retina remain on the same (*ipsilateral*) hemisphere. Consequently, the right hemisphere receives visual information only from the left visual field (from both eyes) and the left hemisphere receives information from the right visual field.

Primary visual cortex

Visual processing in the brain is a complex feat that is achieved through a series of hierarchical processing stages, as well as crosstalk and feedback between brain regions. The primary visual cortex (V1 or striate cortex) is a key structure for visual perception as it is the cortical region where decoding of visual stimuli begins, which will eventually lead to a perceptual experience of the outside world. V1 is located on the most posterior area of the brain (equivalent to Brodmann area 17) and it surrounds the calcarine sulcus, an horizontal fissure in the medial posterior occipital lobe. The visual

information reaches V1 through LGN axonal projections, known as the optic radiation. Studies with patients that suffer from *blindsight syndrome* have suggested that retinal information projects through the LGN and other subcortical structures not only to V1 but also to higher cortex areas; nevertheless, LGN-V1 is the dominant pathway for visual information. The axons relaying information from the superior visual field form a lateral pathway around the temporal lobe – the Meyer's loop – while those conveying information from the inferior visual field extend through the parietal lobe, underneath the cortex. The wiring of these visual pathways are so that V1 has not only a representation of the contralateral visual hemifield, but the upper visual field is mapped on the lower bank of the calcarine sulcus and the lower visual field on the upper bank. The visual representation has yet another particularity – as the foveal region in the retina has an higher density of ganglion cells, its representation in the cortex covers a relatively larger area (it is mapped in the most posterior part of V1, while the peripheral visual field is represented more anteriorly).

The LGN cellular layers send their axons to layer 4 in V1, with the exception of the koniocellular layers, which project into layers 4a in the striate cortex. On the other hand, axons from layer 6 of V1 establish feedback pathway with the LGN. Therefore, the primary visual cortex in each hemisphere is directly connected to its ipsilateral LGN.

The output from V1 primarily follows two major pathways, known as the dorsal and the ventral stream.

- The dorsal stream connects the visual areas V1, V2, dorsomedial area (V6), V5 (MT) and the posterior parietal cortex. This pathway is generally associated with motion, representation of spatial location (it is involved in spatial attention) and eye-hand coordination (e.g., using visual information to position the eyes onto a target and reach for it).
- The ventral stream, on the other hand, consists in a pathway that connects V1 to the visual area V2, then to V4 and to the inferior temporal cortex. Commonly known as the '*what'* stream, it is involved in form recognition and identification/categorization of objects and other visual stimuli. (Farivar et al., 2009).

This *Two-Streams hypothesis* for visual processing was first proposed by Ungerleider and Mishkin, in 1982, and it has been widely accepted. However, there is still much debate regarding the degree of specialization and interconnectivity of these pathways. As stated in a recent study, 'after 25 years, it has become clear that the earlier distinctions in terms of neuroanatomy and functional dissociation are less pure than originally considered' (Mishkin et al., 1982).

Extrastriate cortex

In mammals, the extrastriate cortex is a region located next to the striate cortex in the occipital lobe (equivalent to Brodmann areas 18 and 19). This region includes visual areas V2, V3, V4 and MT and can be associated with an intermediate level of visual processing. Although neurons in the extrastriate cortex still respond strongly to visual stimuli (*lower-level*, from the retina) within their receptive fields, they are modulated by *higher-level* processes that arise from cortical activity, such as attention and working memory. Therefore, throughout the visual cortex, neurons fire (action potentials) when their receptive fields are stimulated, but its response may vary depending on the stimulus; this is known as neuronal tuning. In *lower* visual areas, namely in V1, neurons become more active (fire more frequently) when a simpler visual characteristic is observed (e.g., when a stimulus in a given direction appears in its receptive field). Along the visual pathway, in higher-level areas, neurons present an increasingly complex tuning; the degree of specialization can become such that a neuron in the inferior temporal cortex may fire only when it *sees* a particular face or object.

The extrastriate cortex is involved in the process of translation and interpretation of visual information arriving from V1; for this, it is also known as the visual association area. The first region within this area is V2, which receives feedforward connections from the primary visual cortex, as well as via the pulvinar. V2 is made up of four sub-regions (quadrants), which correspond to the dorsal and ventral representation of this visual field, both in the left and right hemispheres. Despite its functional differences with V1, neurons within V2 still respond to simple visual properties (e.g., orientation and color); nevertheless, they have been shown to be modulated by more complex properties. (Qiu et al., 2005). The following visual area is V3 and it is located immediately in front of V2; to date, its function and cortical extension is still under debate. It is believed that dorsal V3 is part of the dorsal stream, conveying visual information from V1/V2 to the posterior parietal cortex. A recent study has suggested that V3 may be involved in global motion processing (Braddick et al., 2001); however, other researchers do not even consider it to be an independent area, but part of the larger, dorsomedial area (DM). In opposition to its dorsal counterpart, ventral V3 (or VP) is strongly connected with the inferior temporal cortex and less so with V1.

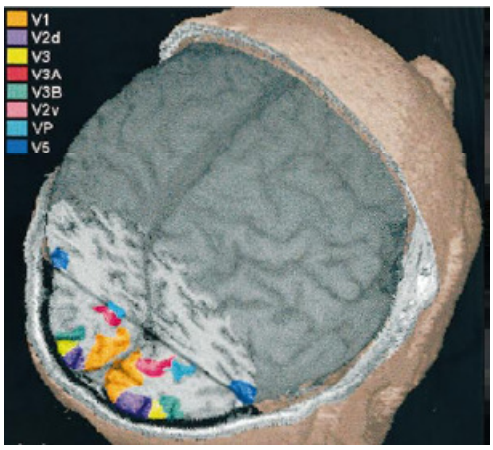

Fig. 6: Three-dimensional reconstruction of the brain; cuts have been made on the occipital lobe to allow visualization of the main visual areas (Smith et al., 1998).

V1 damage functional consequences of scotoma

From early studies to the most recent literature, it has been shown that degeneration or damage caused to the first visual cortical area – V1 – leads to blindness in the corresponding part of the visual field (the cortical representation is damaged). The blind area, or scotoma, is an area in the field of vision where visual acuity is partially diminished or completely lost, surrounded by a field of relatively normal vision. The visual loss occurs in the visual field opposite to the damaged hemisphere and can greatly vary in size. Therefore, it is clear that an impaired V1 significantly limits the flow of visual information from the retina (via LGN) to higher cortical areas. However, it is known that this is not the only visual pathway into the extrastriate areas; these alternative pathways that bypass V1 might be responsible for residual perception reported in patients with *blindsight*, but seem to be insufficient to process and relay the visual information needed for visual awareness.

Retinotopic mapping

From the receptive fields to the visual field maps

A fundamental principle in visual neuroscience is that human perception is inherently connected to the properties of the brain, as its circuits and communication pathways have evolved to recognized and understand the properties of the external world. One of those properties, and perhaps the most important, is space. For instance, we can easily process images with lower or higher contrast, with different colors, even if they are rotated or displaced in some way; but if the spatial organization is tampered, if the 2D or 3D representation of the visual environment is altered, our brain becomes unable to interpret such stimuli as an image and form a visual perception. Therefore, we should expect to find a complex, yet spatially organized representation of the visual field at the cortical level. In fact, visual field (retinotopic) representations appear repeatedly in the cortex, preserving the image features throughout the visual processing pathways. In this way, by retaining a critical image property – spatial organization - the cortical circuitry is able to maintain the information provided by the receptive fields (nearby neurons in the cortex have receptive fields that are close, or even slightly overlaid, in the visual image. And even though they are responsible for interpreting other characteristics of an image (e.g., orientation, motion, color…), different regions of the visual cortex are still wired in a way that a topographical visual field map is preserved.

Historical perspective

As far as in 1881, the occipital lobe was already being linked to vision. For the first time it was suggested that the 'visual center' (of a monkey) was the cortex of his occipital lobe. These findings were possible by studying monkeys with lesions in this part of the cortex, which originated visual alterations (Munk, 1881). Eventually, this visual loss caused by brain lesions was identified and studied in human cases. Two of the most prominent examples were Tatsui Inouye (Japanese ophthalmologist) and Gordon Holmes (British neurologist); their independent studies of neurological cases (mostly due to war injuries), where they found a correlation between the wound location and the visual field loss, unveiled the existence of visual field maps in humans. Furthermore, they have shown that this part of the cortex (V1) had particular traits, such as each hemisphere mapping the contralateral visual hemifield and the foveal area covering comparatively more cortex area than the peripheral visual field – cortical magnification (Holmes, 1918). Later on, additional studies have revealed a multitude of maps; in 1940, electrophysiological studies performed in cats were used to define a second visual area with a spatial mapping (now known as V2), laying next to V1. (Talbot, 1940). A decade later, the same Talbot and Thompson successfully mapped 'visual areas I and II' of the visual cortex in rabbit (Thompson et al., 1950). Then a third area (V3) that surrounds V2 was identified in cat by Hubel and Wiesel, in 1965. The findings of new visual field maps, such as V4 and V5/MT in monkey, followed and evidence of repeated visual field maps throughout the visual cortex grew exponentially. Soon, researchers turned their attention to the organization of those maps and to their role in visual perception.

Some of the first direct observations of the link between vision and the cortex were made by Penfield. Together with Herbert Jasper, this groundbreaking neurosurgeon operated patients with severe epilepsy to destroy nerve cells that were causing seizures. To minimize collateral damage, he electrically stimulated the brain (with the patient only locally anesthetized) and observed the evoked cognitive response. During his extensive efforts to map the human cortex, he found that visual sensations could be produced when the electrical stimulus was applied to certain cortical areas. However, his findings relate mostly to regions outside the striate area (Penfield & Rasmussen, 1952; Penfield & Jasper, 1954). But in 1968, electrical stimuli were applied to the occipital lobe (V1) of a blind man which originated a visual sensation ('phosphene') at the corresponding visual field location; such a discovery was the first milestone of the conceptual idea of developing prosthetic devices that would allow at least a partial recovery from blindness (Brindley & Lewin, 1968).

Retinotopy

Retinotopy can be described has the spatial organization of neuronal activity elicited by visual stimuli. As mentioned above, such organization is a consequence of the spatially specific wiring between the retina and different brain structures (e.g., visual cortex, LGN, pulvinar, etc.); it allows adjacent neurons to have receptive fields that respond to a slightly different part of the visual field. In this way, the visual field is orderly sampled and represented throughout the visual pathways, forming a topographical map of the visual field (or retinotopic map).

Due to this particular functional organization of the visual system, one could expect that visual areas were defined by their retinotopic boundaries; in reality, this has proved to be a more complex task since areas further away from the initial visual processing (V1) do not present complete and organized maps of the visual field. In fact, most of the extrastriate areas are still under debate today as 'of the many areas described by the pioneering mapping studies in monkeys, only two have become universally accepted: the second (V2) and the mediotemporal (MT) areas' (Rosa, 2002). But even in V2, the retinotopic map is considerably more complex than in the striate cortex; adjacent features of visual field may not be represented in adjacent regions of V2. The major disruption in spatial organization derives from the separation of visual information into hemifields: the areas of the retina that respond to the upper visual field are represented in more ventral regions of the extrastriate cortex while those that respond to the lower visual field are represented more dorsally. Based on the topological continuity and the geometric transformations from the visual field to the cortical representation, Rosa classified retinotopic maps as either first-order (V1 and MT) or second-order representations (V2, V3): the former are 'those in which adjacent points of the same hemifield always map to adjacent columns in the contralateral cortex', while in the latter representations the topological equivalence is lost (Rosa, 2002).

Fig. 7: The figure portrays how the left visual field is transformed and represented on the primary visual cortex of the right hemisphere. It is clearly visible that the areas closer to the fovea (face in picture) have a much larger cortical representation (appear to be expanded). The most posterior part of V1 corresponds to the center of the visual field and the image representation is inverted (Wandell et al., 2007).

In a recent study, it has been shown that the visual cortex (in humans and other primates) presents such a marked functional organization that its anatomical development is strongly influenced by its constraints. The cortical sheet presents a folding pattern that is relatively well identified (despite individual variability); what has been found (particularly for V1 and V2) was that the vertical meridian of the visual field is predominantly represented on cortical gyri, while the horizontal meridian is primarily represented on the concave folds of the cortex (sulci). As proposed by the author, this could mean that the retinotopic maps may be influencing the very pattern of cortical folding during brain development (Rajimehr, 2009). Despite the multitude of studies conducted in animals and in human patients (mostly with cortical lesions) that lead to invaluable knowledge, it was only with the advent of fMRI technology (Ogawa and Lee, 1990) that researchers could look into fully functional human visual cortex. The most effective advances in terms of experimental methods and data analysis of human visual field maps measurements were introduced in the mid 90's (Sereno et al., 1995; DeYoe et al., 1996; Engel et al., 1997). Even though these techniques rely on hemodynamic response (which is an indirect measure of neuronal activity that still triggers debate among scientists), there has been an increasing interest in exploring their potential to study the human brain, as well as in the development of clinical applications.

Objectives

This thesis aims to provide more insight in the neurophysiological aspects of optic neuropathies and to explore the possible links between retinal degeneration and visual cortex dysfunction. More precisely, we wanted to assess the structural impact of ganglion cell damage (degeneration of the retina/optic nerve) in cortical cell number, as indexed by cortical thickness of the regions of interest (i.e., visual areas). Additionally, we wanted to understand the level of functional impact of ganglion cell loss in the organization of retinotopic maps. The first part of this work will present data from a group of glaucoma patients, which were subdivided into three groups: ocular hypertension/HTO (subjects that are at risk but have not yet developed the neuropathy), glaucoma suspects (transitional/early stage) and glaucoma (advanced stage of disease). In order to explore and uncover the likely differences between patients in these stages, correlations across global measures (structure-structure and structure-function) are complemented with specific within group analyses. In the second part of this work we will focus on a group of Leber's hereditary optic neuropathy (LHON) patients.

Chapter 2

Methods to study structure and function of visual pathways

Cortical Thickness Analysis (CTA)

Cortical thickness analysis, or CTA, is a neuroimaging technique that allows researchers to look into the structural characteristics of patients and healthy subjects' brains. By using appropriate MRI equipment and data processing software (we have used BrainVoyager QX®), it is possible to obtain the measure of the combined thickness of the 6 cerebral cortex layers. Cortical thickness (CT) throughout one's brain can vary greatly depending on the brain regions and on individual variability, but typical values for the human brain range between 2-4mm (Jones et al., 2000). The study of regional CT variations may provide valuable information about the neuroanatomy and structural alterations that characterize neurodegenerative and neurodevelopmental disorders. For example, normal aging individuals have been shown to have a widespread decrease in CT (Salat et al., 2004), while normal brain development studies have reported interregional statistical associations in CT that may be linked to brain connectivity and its functional networks. Other studies have performed CTA in patients with brain disorders like Alzheimer's disease, where it was observed a pronounced thinning of the cortex, while an increase in cortical thickness was reported in Williams syndrome (Thompson et al., 2005) and in autism (Hardan et al., 2006).
In this study, cortical thickness analysis was performed with BrainVoyager QX through a process that involves four essential steps:

High-quality segmentation of the inner and outer cortex boundary
Starting from high-quality T1-weighted anatomical 3D data sets, this step prepares the data for subsequent thickness measurements. Initially, the raw anatomical output data provided by the MR equipment (Siemens Trio 3T) is converted into data files (DICOM) that can be processed by BrainVoyager. With this software we create a three-dimensional, anatomical representation of the patients' head; subsequently this data undergoes a multitude of processing steps in order to obtain a map of cortical thickness values. Before running the automatic segmentation tools, there are some prerequisites that should be considered:

- The original anatomical 3D data set must have an appropriate spatial resolution (1x1x1mm); if the voxels do not have this exact resolution, an iso-voxel tool should be used to interpolate the data set;
- The contrast between grey matter (GM) and white matter (WM) tissue must be high enough – we use optimized MPRAGE (magnetization prepared rapid acquisition gradient echo) sequences that provide high quality / high contrast

anatomical data); averaging multiple structural scans of the same subject further improves the quality of the data – we used two 9-minute long MPRAGEs for each subject to obtain superior results;

- The intensities across space of the same tissue types should be homogeneous (this can be assessed by looking at the intensity histogram); if the histogram does not show two clearly separated peaks, it is advisable to use the inhomogeneity correction tool (regardless of individual histograms, I have performed this correction of the magnetic field inhomogeneities for all subjects);
- The anatomical data set should be in Talairach space because some tools of the automatic segmentation procedure exploit anatomical knowledge for initial brain segmentation (Talairach masking), filling of ventricles, removing subcortical structures and disconnecting the cortical hemispheres; I have used the spatial transformation tools to convert the original anatomical data sets into Talairach space (see figures at the end of this chapter for a step-by-step overview of data processing).

Cortical thickness measurement in volume space

This step starts with individual segmented cortical hemispheres, where all voxels in the brain have been classified into three types of tissue: WM (light grey), GM (dark grey) and CSF (black); with these files as input, BrainVoyager produces cortex thickness volume maps (VMPs) containing the thickness measures at cortical voxels.

The measurement of cortical thickness, as Jones et al. (2000) point out, is not easy because cortical thickness varies substantially across space; in this case, simple orthogonal measurements (distance from one side of grey matter to the other side) may lead to inaccurate thickness estimates. Therefore, the CT measurements in BrainVoyager QX are based on the Laplace method (Jones et al., 2000).

Cortical thickness measurement in surface space

The created VMPs contain relevant additional information (e.g. gradient maps), which may then be used to efficiently calculate the CT on cortical surface meshes, producing cortex thickness surface maps (SMPs). Although the surface information is identical to what we had in the volume space, it provides an easier access to visualize both sulci and gyri and provides a better view over the entire cortex.

Cortical thickness analysis for regions-of-interest

Cortex thickness values can be calculated for defined patches-of-interest or POIs (e.g., frontal lobe, anterior bank of central sulcus). For this study, the relevant regions are the visual areas of the human visual cortex. Although these areas could be defined based on an anatomical atlas or their relative positions to Brodmann areas, substantial errors would be introduced into the data analysis due to the great anatomical variability among individuals (even though all brains were transformed into the normalized Talairach space). Instead, we have decided to functionally define the visual areas – V1, V2v, VP (ventral) and V2d, V3 (dorsal) – for each subject. For this purpose we have used retinotopic mapping, a method introduced by Sereno and colleagues in 1995.

Tools are available to statistically compare mean regions-of-interest thickness values within a group as well as across groups. However, BrainVoyager requires all subjects' brains to be aligned, a process called cortex-based alignment. Since this method significantly distorts one's brain (while trying to 'align' it with all the others), we have chosen to perform all statistical analysis with SPSS Statistics 18©. There is no automatic feature that allows to export cortical thickness values directly to another platform, so a data sampling was needed. Each visual area was subdivided into three parts – 'foveal', 'intermediate' and 'peripheral' – according to the part of the visual field they encode and for each subdivision 10 CT values were obtained; the subdivision was based on the functional information gathered with an eccentricity paradigm. Therefore, the average cortical thickness of any given visual area was calculated based on 30 different CT values (10+10+10).

In summary, cortical thickness analysis addresses the following main points:

- Measurement of cortical thickness of individual segmented cortical hemispheres (in volume space, VMP, or in surface space, SMP);
- Calculation of individual thickness values in any region-of-interest;
- Statistical analysis that may reveal correlations among CT of visual areas and between CT and other relevant physiological parameters (e.g. retinal thickness, contrast sensitivity).

(For group studies, particularly for whole brain comparisons, it may be relevant to compute average thickness maps across subjects and assess the statistical difference between group maps).

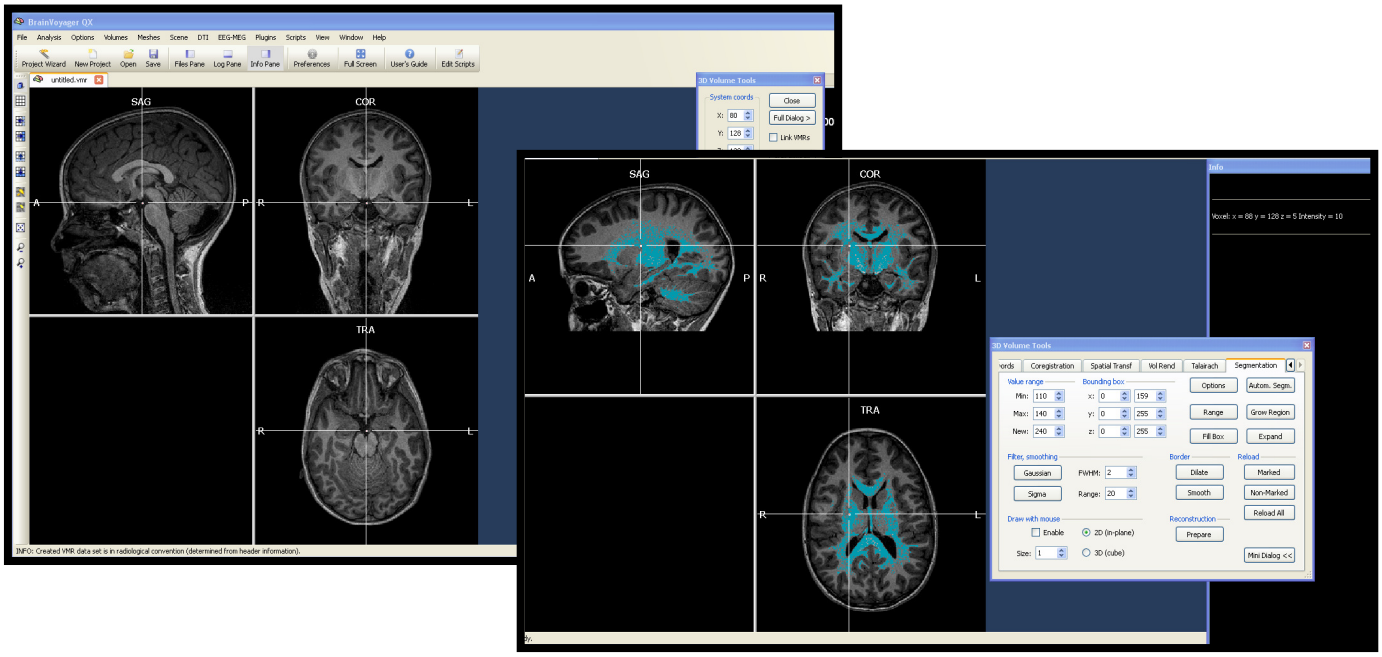

Fig. 8: Original data before processing steps (left); Selection of WM voxels (blue) in order to perform the inhomogeneity correction (right).

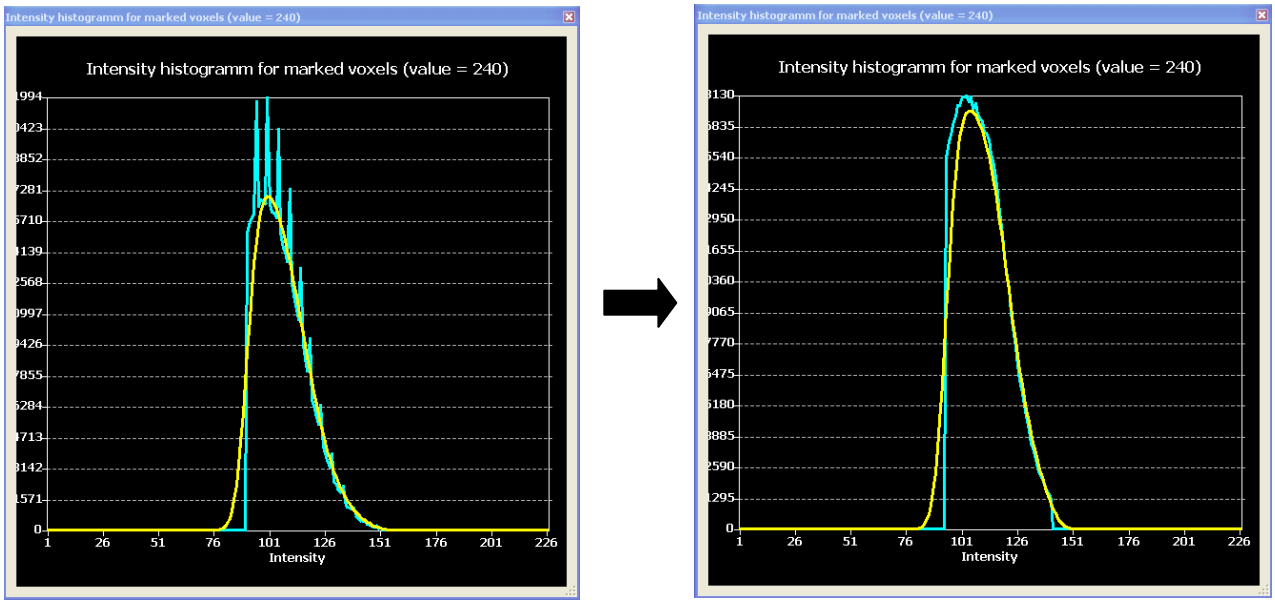

Fig. 9: Histogram of WM voxels before (left) and after (right) the inhomogeneity correction; note that it may be necessary to run the correction algorithm more than once before achieving a smooth, continuous distribution of voxel intensities.

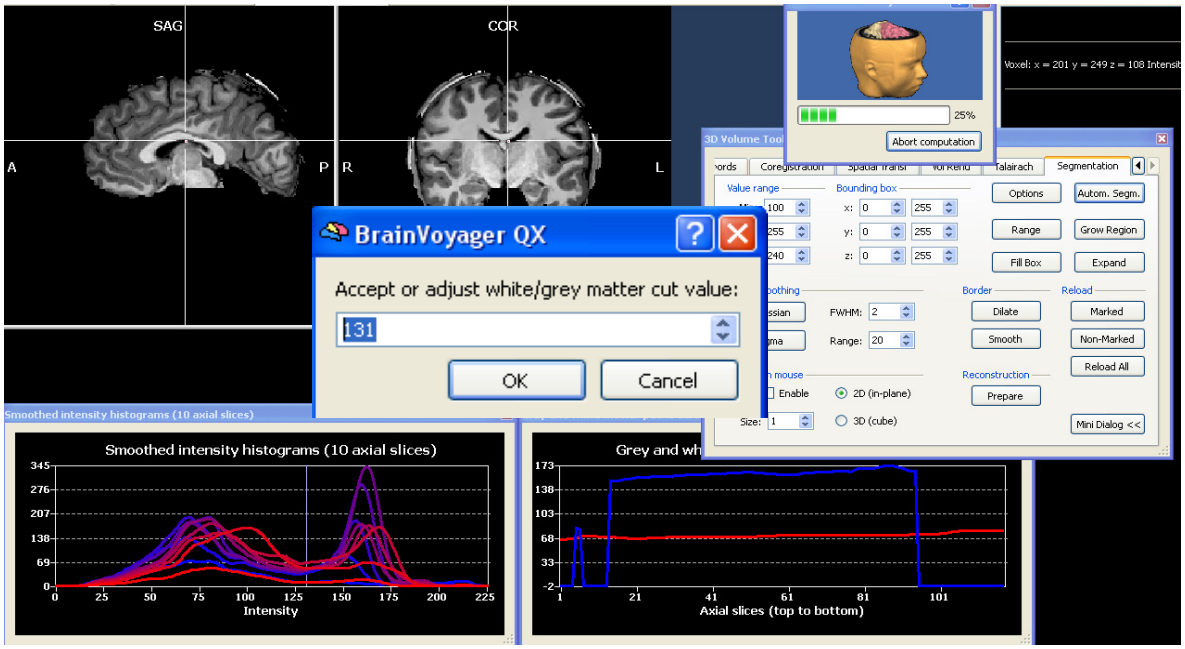

Fig. 10: Automatic segmentation – the WM/GM cut value should be closer to the '*Min*' value of the inhomogeneity correction procedure (lower left side of the WM peak on the histogram) to get the best segmentation possible; the cut point is manually optimized for each individual.

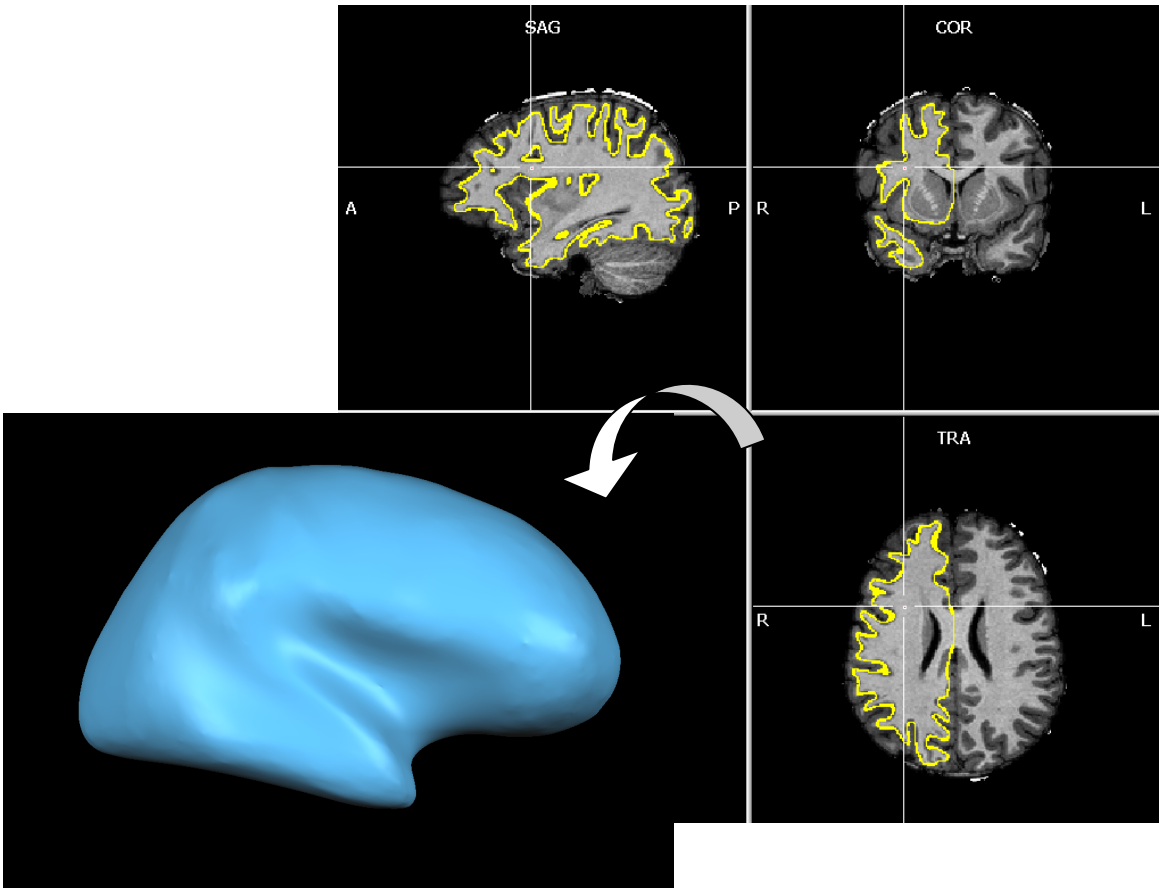

Fig. 11: *RECOSM* surface – WM/GM boundary estimated based on the given cut point (yellow); this boundary is then represented on its own and stretched (or inflated), which will serve as a template where CT maps and retinotopic maps may be overlaid. Inflated *RECOSM* surface of a subject's right hemisphere (blue).

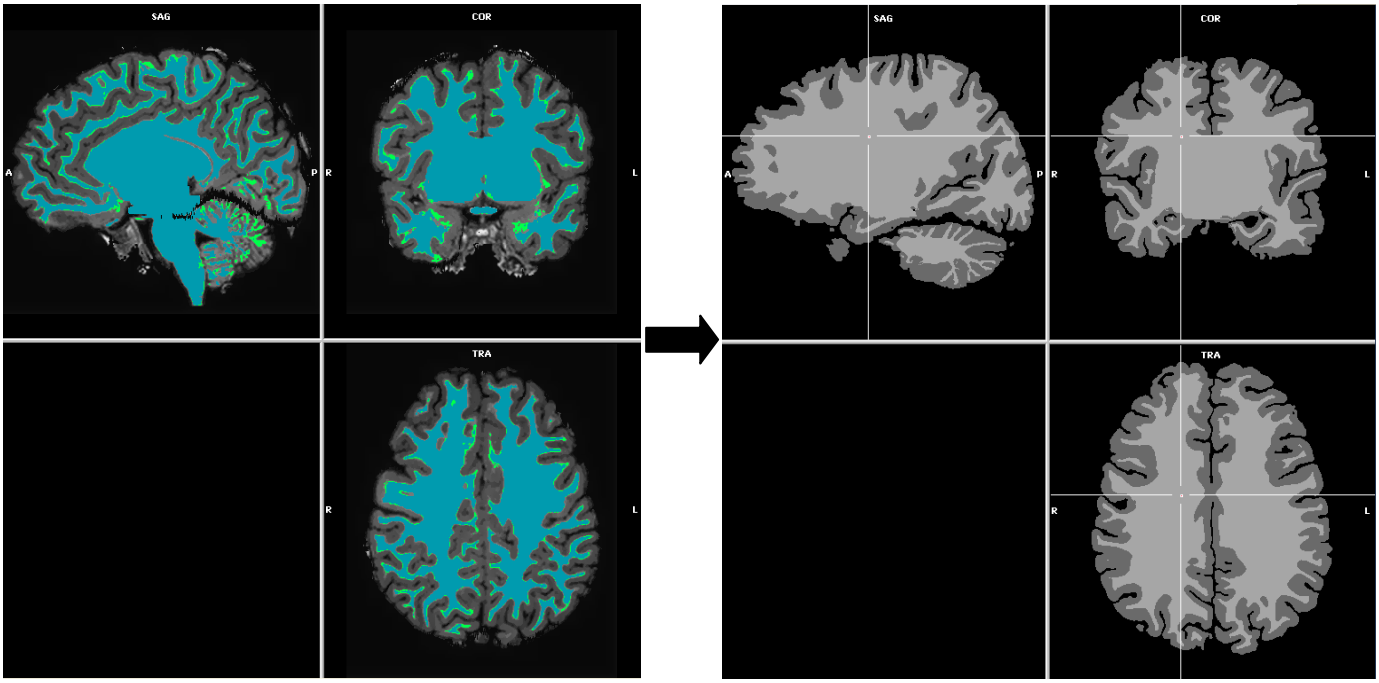

Fig. 12: Final preparations for cortical thickness measurements; the white matter is increasingly selected by adjusting global and local WM-GM cut points (blue and green voxels, respectively). The result (right) is a complete segmentation and classification of brain tissue into three types: WM (light grey), GM (dark grey) and CSF/background (black).

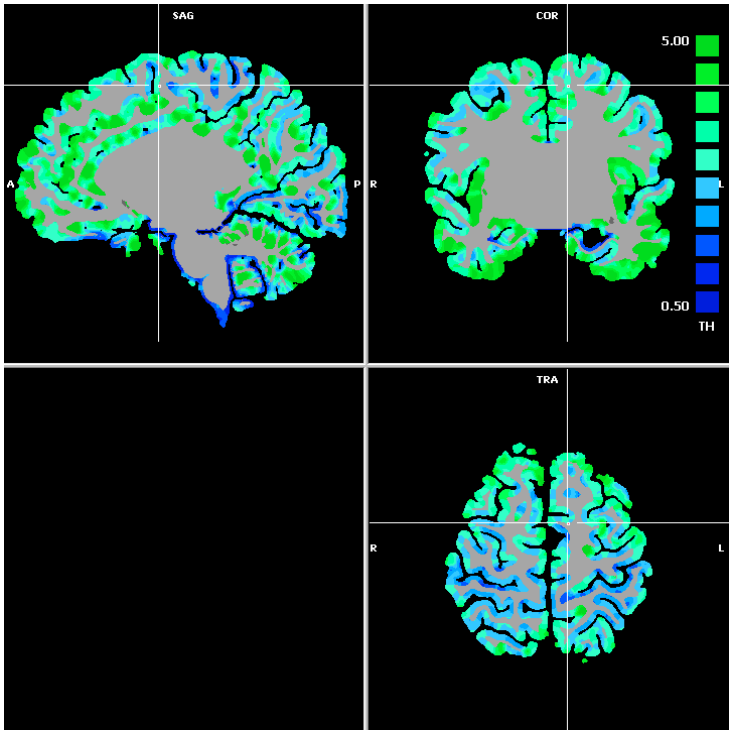

Fig. 13: Cortical thickness measurement in individual brain; the resulting file is a volume map (VMP) file containing submaps with the cortical thickness estimates, gradients and other parameters used for CT calculation. The cortical thickness map appears superimposed on the VMR data (color scale: dark blue – 0.5mm, light blue – 2/3 mm, green – 5 mm).

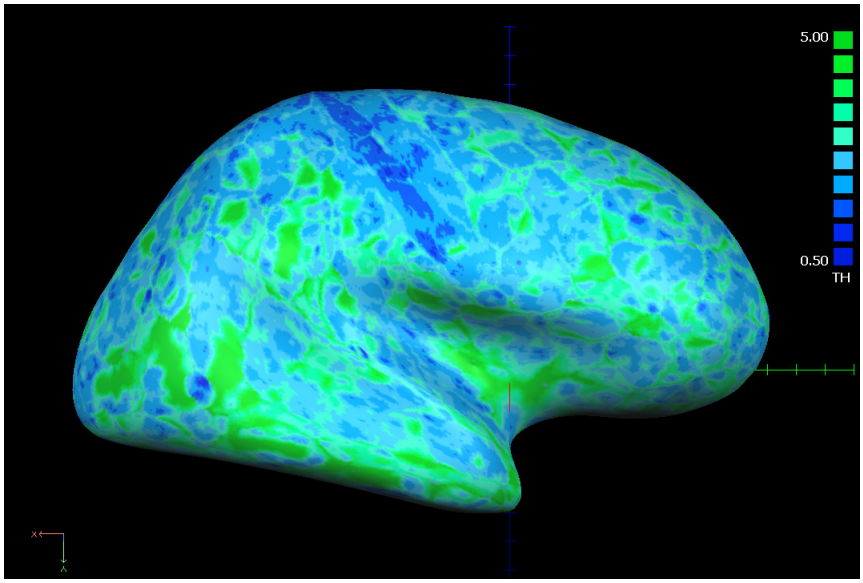

Fig. 14: Cortical thickness map in surface space (SMP); the VMP is stretched to fit an inflated representation (*RECOSM* mesh) of a subject's right hemisphere.

Methods in Retinotopy

Retinotopy is the functional organization of the visual cortex that relies on the topographically preserved projections from the retina to the LGN layers and then to V1. With proper fMRI stimuli we can map visual areas in the human brain (as introduced by Sereno *et al.,* 1995), since peak activation in adjacent areas alternate with a mirror / non-mirror representation of the visual field that correspond to the horizontal and vertical meridians. All subjects in this study have undergone the same imaging sequence protocol: MPRAGE T1-weighted, three polar angle functional paradigms, one eccentricity functional paradigm and a second MPRAGE T1-weighted. The 3T scanner (Siemens Trio 3T) was set with the following parameters: TR = 2000 ms, TE = 39 ms, interslice time = 76 ms, voxel size = 2 x 2 x 2 mm (for functional data), FOV = 256 mm x 256 mm, slice thickness = 2 mm, number of slices = 26, imaging matrix = 128 x 128. The visual stimuli presented in real-time to the subjects were computer delivered and a mirror was used to reflect the image on a screen while the subject was lying inside the scanner. The polar angle and eccentricity experiments, i.e., a rotating checkerboard wedge stimulus and an expanding ring stimulus, respectively, stimulate the visual field repeatedly whilst the subject fixates a spot (yellow dot) in the center of the image. Each functional stimulus lasts for just over three minutes and comprises four complete cycles (rotations or expansion) of 48s each. These experiments, also known as *phase-encoding,* result in the mapping of the horizontal and vertical meridians that allow the manual delineation of the visual areas in the human visual cortex.

Fig. 15: Rotating wedge or polar angle stimulus (left); expanding ring or eccentricity stimulus (right). Both stimuli have a rapidly flickering checkerboard pattern.

To perform the mapping, the background circle (that represents the visual field) was divided into 8 areas that were used to define the functional protocol with BrainVoyager. To delineate the visual areas, the data was processed as described in the software documentation, based on the retinotopic mapping experiments performed by Goebel and colleagues, in 1998. In terms of data pre-processing, the most relevant procedures include mean intensity adjustment (to reduce variation of mean signal intensity across volumes), slice scan time correction (a temporal offset introduced by the MR data acquisition), 3D motion correction (head movements) and spatial and temporal smoothing and filtering. To achieve higher statistical significance, we have combined the three polar angle data sets into a single volume time course (VTC) file. To do so, we had to ensure that all data sets were precisely aligned among each other and also aligned with the anatomical data. All the alignment procedures we used are fully automatic in order to achieve optimal, unbiased results.

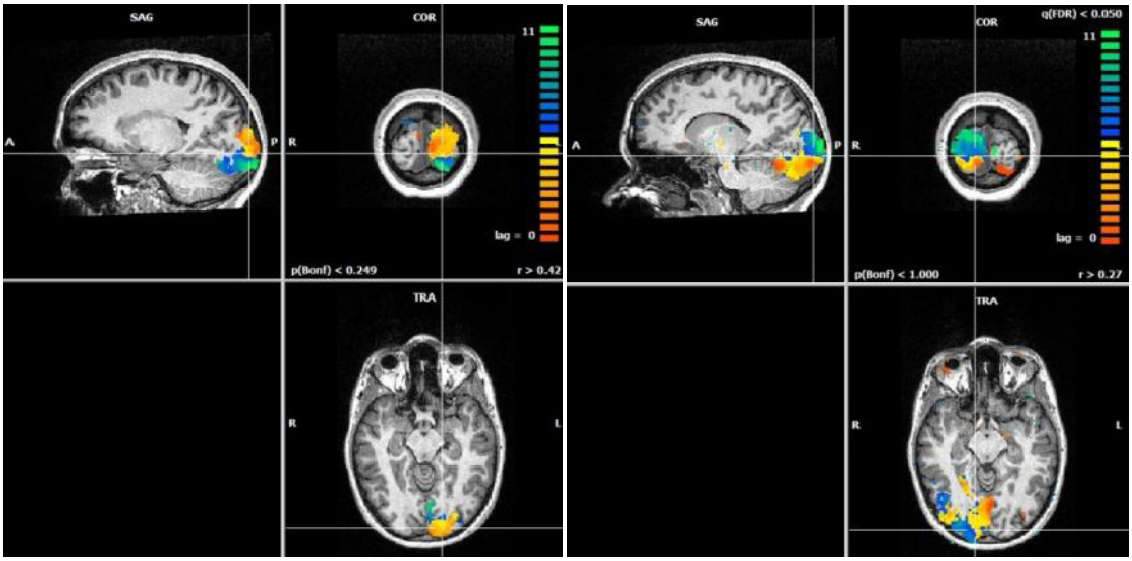

Fig. 16: Retinotopic map of the left and right visual cortex (on the left and right, respectively). These maps represent a computation of the linear correlation of activity in the various visual areas (such computation has the average VTC data files as input).

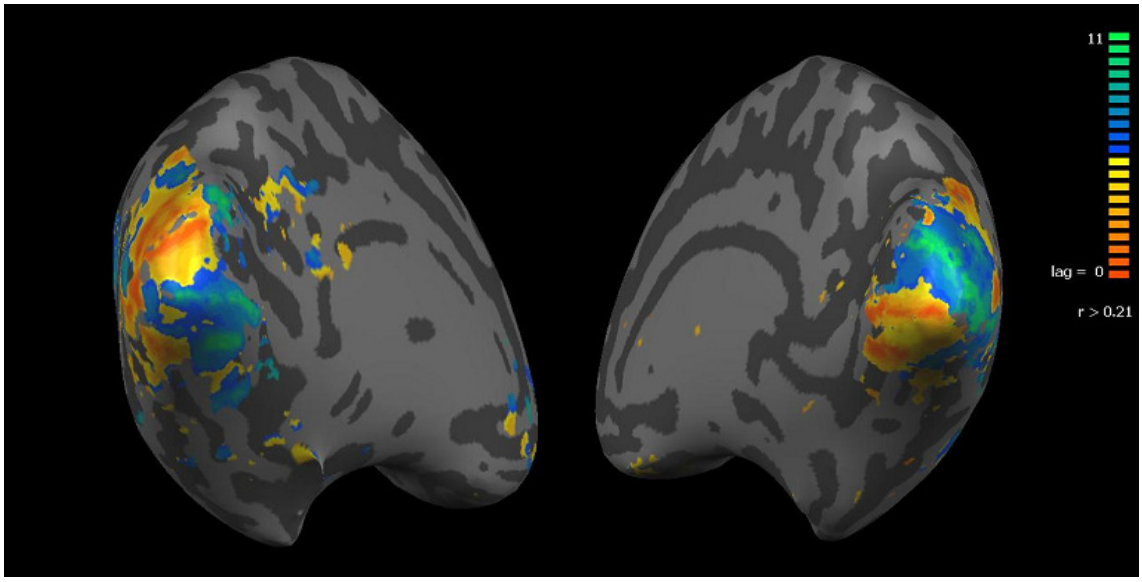

Fig. 17: Retinotopic (polar angle-based) maps for both hemispheres in surface space (above); mirror / non-mirror reflections are clearly visible ventrally and dorsally of the calcarine sulcus. Eccentricity maps (below) reveal that central regions of the visual field are represented in more posterior areas of the visual cortex (warm colors) while peripheral regions are encoded more anteriorly (cool colors).

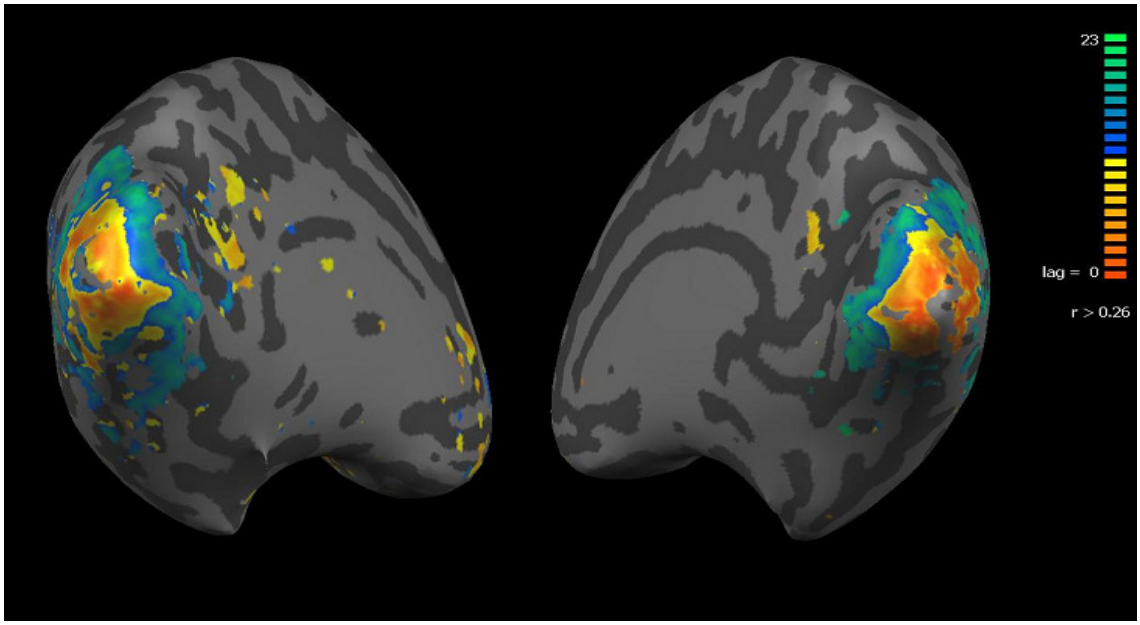

Retinal and RNFL thickness measurements

Optical Coherence Tomography (OCT) is a popular technique for assessing the patients' retinal and RNFL thickness in real-time. It provides high-resolution, cross-sectional images of retinal tissue based on optical interferometry using infra-red and low coherence light, with longitudinal resolution of approximately 10 µm (Hee *et al.*,

1995). Besides having a superior resolution, OCT is also a quantitative, non-invasive method that has been used in the diagnosis of a variety of diseases of the macula and the optic nerve. Reduction of RNFL thickness, measured by OCT, correlates with increased severity of RNFL damage as assessed photographically and histologically in studies with primates. OCT RNFL measures have been shown to decrease with age, as well as with increasing severity/progression of glaucoma (Porciatti et al., 2006). While for the glaucoma studied we have used the OCT Stratus equipment, all Leber's Neuropathy subjects were screened using the OCT Spectralis. This new equipment offers a superior resolution than its predecessor and has a better signal to noise ratio. Additionally, the acquisition process is much faster as the data is presented on the Fourier space.

Methods to study visual function in retinocortical disease

FDT – Perimetry as a method to study retinotopy behaviorally

The Frequency Doubling Technology (FDT) perimeter is an instrument designed for fast and effective detection of visual field loss. Previous studies have demonstrated its high sensitivity and specificity in the detection of early glaucomatous damage, as well as in other ocular, retinal and neurological disorders (Johnson et al., 1997). Among the advantages of FDT there is the fact that it is easy to administer and interpret, it is patient-friendly, it is hardly affected by refractive error and cataract and it is fast and highly reliable (test-retest).

FDT perimetry is based on a phenomenon described four decades ago; it was then observed that when an achromatic sinusoidal grating of low spatial frequency undergoes counter-phased flickering at a high temporal frequency (>7 Hz), the apparent spatial frequency of the grating appears to double (Kelly, 1966). This nonlinear response of the visual system has been thought to be due to the appearance of a second-harmonic distortion that may involve rectification and response compression (Kelly, 1981).

Maddess and Henry reported that the FD illusion could be useful in detecting glaucomatous field loss. The FDT stimulus is thought to predominantly stimulate the magnocellular ganglion cell pathway, which is primarily involved in motion and flicker detection. Some suggested that the neurophysiological explanation for the frequency doubling illusion in humans lies in a subgroup of M cells (the M_y cells); these are thought to be preferentially lost in early glaucoma (Maddess and Henry, 1992).

The use of FDT perimetry in a clinical setting began just over a decade ago, thus further longitudinal studies are needed to evaluate the role of FDT in monitoring progressive field loss, its effectiveness in predicting glaucomatous defects and the possible correlations it has to structural loss.

Standard Automated Perimetry (SAP)

Visual Perimetry is a psychophysical procedure that provides a quantitative estimate of the function of the visual field. The most common test of functional vision used in clinical diagnosis and evaluation of glaucomatous stages is the static-threshold, computer-automated perimetry or Standard Automated Perimetry (SAP), which uses standard stimulus conditions and psychophysical approaches. In static perimetry, the size and location of the test target remain constant, while the intensity of a fixed target varies in order to determine the sensitivity of specific VF locations; in sum, SAP measures the retinal sensitivity at predetermined locations in the visual field (Punjabi, 2006). On the Octopus perimeter (used in this study), the intensity of the supra-threshold stimulus is based on data from age-matched normal subjects. Despite the advantages of this functional measure, substantial ganglion cell damage can take place before SAP detects functional deficits, so we should use caution when taking conclusions from a lack of structure-function correlations.

Global measures

FDT provides two global indexes to generally summarize the visual field results for threshold tests: mean deviation, MD, and pattern standard deviation, PSD (they are both expressed in dB). On one hand, MD represents the average sensitivity deviation from a normal healthy person of the same age; it is an indication of the overall VF sensitivity and can either be a negative or positive value depending on whether the individual's general contrast sensitivity is below or above the average for that same age group. On the other hand, PSD gives an indication of how each test location deviates from the age adjusted data. It represents how evenly the field loss is spread across the VF, thus it is indicative of localized loss. A null PSD means that the individual VF has no deviation from a height adjusted VF profile of a normal person of the same age; a higher the PSD value reveals a greater amount of irregularities in the VF.

For the SAP, the global measures are MD and LV (the latter is a measure identical to the pattern standard deviation, PSD).

Chapter 3

Results

Structural and structure-function correlations

Glaucoma (1st part of the study)

Cortical thickness of retinotopic areas

The table below presents all CT measurements used during this part of the study; all values are in millimeters. 21 subjects were evaluated by an experienced ophthalmologist and divided into three groups: Ocular hypertension / HTO (n=9), Glaucoma suspect / GS (n=8) and Glaucoma, G (n=4). In terms of CT of visual areas, there are six rows of data for each subject (ID) – foveal, intermediate and peripheral sub-regions, for both hemispheres. *Average* values were calculated for each sub-region; *total* values were obtained for each region by averaging the three corresponding sub-regions.

ID	Age	Sex	Group	Hemisphere	V1 avg	V1 total	V2v avg	V2v tot.	VP avg	VP tot.	V2d avg	V2d tot.	V3 avg	V3 tot.
19580400317	51	F	G	LH - fovea	**2,05**	**2,23**	**2,67**	**2,67**	**2,76**	**2,54**	**2,54**	**2,56**	**2,21**	**2,18**
19580400317	51	F	G	LH - inter.	**2,7**		**3,02**		**2,44**		**2,67**		**2,55**	
19580400317	51	F	G	LH - perif.	**1,95**		**2,33**		**2,42**		**2,48**		**1,79**	
19580400317	51	F	G	RH - fovea	**1,91**	**2,23**	**2,33**	**2,18**	**2,33**	**2,25**	**2,48**	**2,49**	**2,23**	**2,30**
19580400317	51	F	G	RH - inter.	**2,79**		**2,33**		**2,15**		**2,27**		**2,04**	
19580400317	51	F	G	RH - perif.	**1,99**		**1,89**		**2,27**		**2,71**		**2,63**	
19521100609	57	F	G	LH - fovea	**1,97**	**2,26**	**2,03**	**2,16**	**2,23**	**2,15**	**1,94**	**2,00**	**1,98**	**2,03**
19521100609	57	F	G	LH - inter.	**2,4**		**2,20**		**2,00**		**1,92**		**2,00**	
19521100609	57	F	G	LH - perif.	**2,4**		**2,26**		**2,22**		**2,13**		**2,11**	
19521100609	57	F	G	RH - fovea	**2,02**	**2,40**	**1,92**	**2,30**	**2,38**	**2,31**	**2,20**	**2,07**	**2,40**	**2,06**
19521100609	57	F	G	RH - inter.	**2,95**		**2,65**		**2,49**		**2,00**		**1,80**	
19521100609	57	F	G	RH - perif.	**2,23**		**2,32**		**2,06**		**2,00**		**1,98**	
19381100600	71	F	G	LH - fovea	**2,34**	**2,34**	**2,38**	**2,11**	**2,05**	**2,10**	**1,90**	**2,03**	**2,13**	**2,22**
19381100600	71	F	G	LH - inter.	**2**		**2,05**		**1,97**		**2,20**		**2,31**	
19381100600	71	F	G	LH - perif.	**2,68**		**1,91**		**2,28**		**1,99**		**2,21**	
19381100600	71	F	G	RH - fovea	**2,42**	**2,54**	**2,78**	**2,54**	**2,37**	**2,12**	**2,09**	**2,15**	**2,04**	**2,00**
19381100600	71	F	G	RH - inter.	**2,47**		**2,33**		**1,87**		**2,00**		**1,88**	
19381100600	71	F	G	RH - perif.	**2,72**		**2,50**		**2,13**		**2,36**		**2,07**	
19460900883	63	F	G	LH - fovea	**1,88**	**2,06**	**1,99**	**1,99**	**1,94**	**1,92**	**1,63**	**1,91**	**1,86**	**1,98**
19460900883	63	F	G	LH - inter.	**2,37**		**2,25**		**1,90**		**2,16**		**2,15**	
19460900883	63	F	G	LH - perif.	**1,92**		**1,74**		**1,91**		**1,94**		**1,94**	
19460900883	63	F	G	RH - fovea	**2,02**	**2,01**	**2,09**	**2,07**	**1,94**	**2,05**	**1,95**	**1,96**	**2,31**	**2,08**
19460900883	63	F	G	RH - inter.	**2,12**		**2,02**		**2,12**		**2,27**		**2,06**	
19460900883	63	F	G	RH - perif.	**1,89**		**2,11**		**2,10**		**1,66**		**1,88**	
19660600035	43	F	GS	LH - fovea	**1,95**	**1,97**	**2,35**	**2,27**	**2,35**	**2,28**	**2,38**	**2,09**	**2,08**	**2,29**
19660600035	43	F	GS	LH - inter.	**1,9**		**2,26**		**2,44**		**2,06**		**2,58**	
19660600035	43	F	GS	LH - perif.	**2,07**		**2,19**		**2,06**		**1,84**		**2,21**	
19660600035	43	F	GS	RH - fovea	**1,74**	**1,99**	**1,96**	**1,82**	**2,14**	**2,00**	**2,17**	**1,94**	**2,16**	**2,12**
19660600035	43	F	GS	RH - inter.	**2,38**		**1,70**		**1,94**		**1,92**		**2,18**	
19660600035	43	F	GS	RH - perif.	**1,86**		**1,80**		**1,91**		**1,72**		**2,03**	
19350300928	75	M	GS	LH - fovea	**1,91**	**1,89**	**2,22**	**1,92**	**1,89**	**2,00**	**1,96**	**2,11**	**2,40**	**2,31**

19350300928	75	M	GS	LH - inter.	1,76		1,69		2,10		2,15		2,36	
19350300928	75	M	GS	LH - perif.	2		1,84		2,01		2,21		2,18	
19350300928	75	M	GS	RH - fovea	1,86	1,99	1,79	2,01	1,70	2,15	1,51	1,99	2,05	2,46
19350300928	75	M	GS	RH - inter.	2,09		2,47		2,49		2,28		2,55	
19350300928	75	M	GS	RH - perif.	2,01		1,78		2,26		2,17		2,77	
19550300128	55	F	GS	LH - fovea	2,08	2,33	2,01	2,03	2,34	2,02	2,26	2,16	2,17	2,29
19550300128	55	F	GS	LH - inter.	2,38		2,09		1,88		1,96		1,91	
19550300128	55	F	GS	LH - perif.	2,53		2,00		1,84		2,26		2,79	
19550300128	55	F	GS	RH - fovea	2,15	2,39	2,87	2,37	1,99	2,41	2,04	2,24	2,27	2,13
19550300128	55	F	GS	RH - inter.	2,49		2,25		3,18		2,20		1,84	
19550300128	55	F	GS	RH - perif.	2,53		2,00		2,06		2,49		2,28	
19510800677	58	F	GS	LH - fovea	2,04	2,27	2,46	2,43	2,36	2,27	2,75	2,31	2,00	2,22
19510800677	58	F	GS	LH - inter.	2,33		2,21		2,23		2,20		2,19	
19510800677	58	F	GS	LH - perif.	2,43		2,62		2,21		1,97		2,47	
19510800677	58	F	GS	RH - fovea	2,59	2,42	2,51	2,35	2,17	2,19	2,70	2,55	2,07	2,17
19510800677	58	F	GS	RH - inter.	2,35		1,96		2,26		2,75		2,44	
19510800677	58	F	GS	RH - perif.	2,33		2,57		2,13		2,20		2,00	
19560600861	53	M	GS	LH - fovea	2,04	2,10	2,26	2,20	2,04	2,06	2,13	1,94	1,93	2,04
19560600861	53	M	GS	LH - inter.	1,97		2,14		1,91		2,01		2,08	
19560600861	53	M	GS	LH - perif.	2,28		2,20		2,24		1,67		2,10	
19560600861	53	M	GS	RH - fovea	1,96	2,00	2,09	2,01	1,89	2,16	2,12	1,99	1,81	2,00
19560600861	53	M	GS	RH - inter.	2,26		1,88		2,15		1,84		2,05	
19560600861	53	M	GS	RH - perif.	1,79		2,06		2,45		2,01		2,15	
19430200515	67	M	GS	LH - fovea	2,43	2,24	2,09	2,06	1,95	1,94	2,54	2,50	2,02	1,97
19430200515	67	M	GS	LH - inter.	2		2,16		1,88		2,17		1,95	
19430200515	67	M	GS	LH - perif.	2,28		1,93		1,98		2,80		1,93	
19430200515	67	M	GS	RH - fovea	2,19	2,28	1,88	2,35	2,10	2,45	1,96	2,21	2,04	2,20
19430200515	67	M	GS	RH - inter.	2,61		2,71		2,55		2,09		2,51	
19430200515	67	M	GS	RH - perif.	2,05		2,45		2,71		2,59		2,06	
19460400145	63	F	GS	LH - fovea	2,2	2,36	2,05	2,13	2,23	2,29	2,07	2,21	2,15	2,15
19460400145	63	F	GS	LH - inter.	2,42		2,13		2,26		2,30		2,39	
19460400145	63	F	GS	LH - perif.	2,45		2,21		2,39		2,27		1,90	
19460400145	63	F	GS	RH - fovea	2,3	2,33	1,95	1,88	2,16	2,12	2,33	2,23	2,27	2,26
19460400145	63	F	GS	RH - inter.	2,56		1,82		2,16		2,17		2,19	
19460400145	63	F	GS	RH - perif.	2,14		1,86		2,03		2,19		2,32	
19470800085	62	M	GS	LH - fovea	2,26	2,28	2,66	2,43	2,25	2,46	2,18	2,36	2,09	2,11
19470800085	62	M	GS	LH - inter.	2,51		2,69		2,85		2,55		1,88	
19470800085	62	M	GS	LH - perif.	2,07		1,95		2,27		2,34		2,36	
19470800085	62	M	GS	RH - fovea	2,52	2,30	2,20	2,05	2,10	2,05	2,37	2,47	2,09	2,02
19470800085	62	M	GS	RH - inter.	2,14		1,89		2,16		2,57		1,97	
19470800085	62	M	GS	RH - perif.	2,25		2,07		1,90		2,46		2,01	
19391200175	70	M	HTO	LH - fovea	1,96	2,49	1,65	1,94	1,99	1,88	1,79	1,85	1,88	1,87
19391200175	70	M	HTO	LH - inter.	2,84		2,08		1,90		1,90		1,84	
19391200175	70	M	HTO	LH - perif.	2,66		2,08		1,76		1,87		1,88	
19391200175	70	M	HTO	RH - fovea	2,16	2,42	1,69	1,89	1,74	1,90	1,72	1,88	2,00	1,93
19391200175	70	M	HTO	RH - inter.	3,1		1,98		1,85		2,08		1,83	
19391200175	70	M	HTO	RH - perif.	2		2,00		2,12		1,85		1,97	
19541200494	55	M	HTO	LH - fovea	2,29	2,06	2,30	2,06	2,15	2,19	2,29	2,03	1,94	2,15
19541200494	55	M	HTO	LH - inter.	1,92		1,97		2,35		2,02		2,46	
19541200494	55	M	HTO	LH - perif.	1,96		1,92		2,06		1,78		2,04	
19541200494	55	M	HTO	RH - fovea	2,03	1,92	2,01	2,35	2,20	2,06	2,05	2,31	1,94	2,04
19541200494	55	M	HTO	RH - inter.	1,8		2,45		1,92		2,41		2,17	

19541200494	55	M	HTO	RH - perif.	**1,94**		**2,59**		**2,06**		**2,48**		**2,02**	
19570100748	53	F	HTO	LH - fovea	**2,1**	**2,32**	**2,58**	**2,18**	**2,35**	**2,17**	**1,68**	**2,00**	**2,46**	**2,03**
19570100748	53	F	HTO	LH - inter.	**2,74**		**1,85**		**2,09**		**2,12**		**1,77**	
19570100748	53	F	HTO	LH - perif.	**2,12**		**2,12**		**2,07**		**2,21**		**1,87**	
19570100748	53	F	HTO	RH - fovea	**2,13**	**2,12**	**2,32**	**2,16**	**2,17**	**2,17**	**1,90**	**1,91**	**2,19**	**2,04**
19570100748	53	F	HTO	RH - inter.	**1,95**		**2,10**		**2,06**		**1,83**		**1,97**	
19570100748	53	F	HTO	RH - perif.	**2,29**		**2,05**		**2,28**		**2,01**		**1,95**	
19461000557	63	F	HTO	LH - fovea	**2,15**	**2,24**	**2,09**	**1,98**	**2,27**	**2,16**	**1,77**	**1,86**	**2,31**	**2,29**
19461000557	63	F	HTO	LH - inter.	**2,27**		**1,96**		**2,13**		**1,78**		**2,33**	
19461000557	63	F	HTO	LH - perif.	**2,3**		**1,88**		**2,08**		**2,02**		**2,22**	
19461000557	63	F	HTO	RH - fovea	**2,01**	**2,07**	**1,99**	**1,90**	**2,09**	**2,09**	**1,80**	**1,79**	**2,00**	**2,17**
19461000557	63	F	HTO	RH - inter.	**2,12**		**1,91**		**2,04**		**1,86**		**2,34**	
19461000557	63	F	HTO	RH - perif.	**2,07**		**1,80**		**2,13**		**1,71**		**2,16**	
19550100742	55	M	HTO	LH - fovea	**1,83**	**1,97**	**1,83**	**1,90**	**2,16**	**2,02**	**2,04**	**2,06**	**1,81**	**2,02**
19550100742	55	M	HTO	LH - inter.	**1,94**		**2,07**		**1,96**		**2,00**		**2,02**	
19550100742	55	M	HTO	LH - perif.	**2,15**		**1,80**		**1,95**		**2,14**		**2,23**	
19550100742	55	M	HTO	RH - fovea	**1,78**	**2,00**	**1,99**	**2,00**	**1,93**	**2,11**	**1,75**	**1,76**	**1,97**	**1,93**
19550100742	55	M	HTO	RH - inter.	**2,1**		**1,86**		**2,08**		**1,78**		**2,08**	
19550100742	55	M	HTO	RH - perif.	**2,12**		**2,15**		**2,31**		**1,74**		**1,75**	
19500600240	59	M	HTO	LH - fovea	**2,23**	**2,20**	**2,20**	**2,17**	**2,42**	**2,24**	**2,13**	**2,10**	**2,03**	**2,19**
19500600240	59	M	HTO	LH - inter.	**2,38**		**2,05**		**2,16**		**1,96**		**2,44**	
19500600240	59	M	HTO	LH - perif.	**2**		**2,25**		**2,15**		**2,20**		**2,11**	
19500600240	59	M	HTO	RH - fovea	**2,21**	**2,36**	**2,23**	**2,09**	**2,16**	**2,13**	**1,88**	**2,15**	**2,08**	**2,18**
19500600240	59	M	HTO	RH - inter.	**2,61**		**2,01**		**2,05**		**2,14**		**2,16**	
19500600240	59	M	HTO	RH - perif.	**2,27**		**2,03**		**2,17**		**2,44**		**2,29**	
19390500171	71	M	HTO	LH - fovea	**2,01**	**2,26**	**2,29**	**2,24**	**2,19**	**2,13**	**2,36**	**2,22**	**2,74**	**2,40**
19390500171	71	M	HTO	LH - inter.	**2,46**		**2,08**		**1,85**		**2,15**		**2,28**	
19390500171	71	M	HTO	LH - perif.	**2,3**		**2,34**		**2,34**		**2,15**		**2,18**	
19390500171	71	M	HTO	RH - fovea	**2,14**	**2,35**	**2,18**	**2,19**	**2,02**	**2,00**	**2,11**	**2,41**	**2,34**	**2,48**
19390500171	71	M	HTO	RH - inter.	**2,69**		**2,29**		**2,05**		**2,49**		**2,41**	
19390500171	71	M	HTO	RH - perif.	**2,22**		**2,10**		**1,94**		**2,64**		**2,68**	
19490200369	61	F	HTO	LH - fovea	**2,22**	**2,03**	**2,25**	**2,00**	**1,93**	**2,08**	**2,27**	**2,20**	**2,06**	**2,16**
19490200369	61	F	HTO	LH - inter.	**2,2**		**1,99**		**2,12**		**2,05**		**2,30**	
19490200369	61	F	HTO	LH - perif.	**1,66**		**1,77**		**2,18**		**2,28**		**2,12**	
19490200369	61	F	HTO	RH - fovea	**2,13**	**2,08**	**2,17**	**2,23**	**2,10**	**2,00**	**2,09**	**2,28**	**1,95**	**2,14**
19490200369	61	F	HTO	RH - inter.	**2,03**		**2,05**		**1,87**		**2,41**		**2,17**	
19490200369	61	F	HTO	RH - perif.	**2,07**		**2,47**		**2,02**		**2,34**		**2,29**	
19501200262	59	M	HTO	LH - fovea	**2,16**	**2,13**	**2,16**	**2,38**	**2,55**	**2,47**	**2,04**	**2,11**	**2,62**	**2,52**
19501200262	59	M	HTO	LH - inter.	**2,15**		**2,55**		**2,70**		**2,27**		**2,45**	
19501200262	59	M	HTO	LH - perif.	**2,09**		**2,42**		**2,17**		**2,03**		**2,50**	
19501200262	59	M	HTO	RH - fovea	**2,15**	**2,45**	**2,24**	**2,11**	**2,08**	**1,95**	**2,48**	**2,24**	**1,96**	**2,02**
19501200262	59	M	HTO	RH - inter.	**2,6**		**2,11**		**2,03**		**2,15**		**1,89**	
19501200262	59	M	HTO	RH - perif.	**2,6**		**1,97**		**1,74**		**2,10**		**2,22**	

Table 1: Values of cortical thickness for individual visual areas (HTO, GS and G subjects).

Correlations between thickness of retinotopic areas and retinal nerve fiber layer of the optic nerve (RNFL)

To calculate correlations between the cortical thickness of visual areas and the RNFL of the optic nerve we have used parametric statistics (Pearson Correlation coefficient). The analysis was performed using all data (CT from both hemisphere) and separately for each hemisphere. Furthermore, both global (HTO+GS+G) and within group correlations were performed. All variables follow a normal distribution (Kolmogorov-Smirnov test, $p>0.01$), with the exception for the glaucoma (G) group when hemispheres are analyzed separately ($n=4$); in this case, the variables follow a normal distribution according to the Shapiro-Wilk test, but we decided to complement the analysis with non-parametric correlations (Spearman coefficient).

HTO+GS+G (LH+RH)	Pearson Correlation	Sig. (2-tailed)	N
V2v – VP	.697	.000	42
V2v – V2d	.544	.000	42
VP – V3	.358	.020	42
RNFL Sup – RNFL Inf	.757	.000	42
RNFL Sup – RNFL Nasal	.401	.008	42
RNFL Inf – RNFL Nasal	.660	.000	42

HTO (LH+RH)	Pearson Correlation	Sig. (2-tailed)	N
V2v – VP	.510	.030	18
V2v – V2d	.645	.004	18
V2v – V3	.516	.028	18
VP – V3	.583	.011	18
V3 – RNFL Sup	-0.606	.008	18

GS (LH+RH)	Pearson Correlation	Sig. (2-tailed)	N
V1 – V2d	.717	.002	16
V2v – VP	.774	.000	16
RNFL Sup – RNFL Inf	.709	.002	16
RNFL Inf – RNFL Nasal	.591	.016	16

G (LH+RH)	Pearson Correlation	Sig. (2-tailed)	N
V2v – VP	.775	.024	8
VP – V2d	.814	.014	8
VP – RNFL Inf	.750	.032	8
RNFL Sup – RNFL Inf	.969	.000	8
RNFL Sup – RNFL Nasal	.742	.035	8
RNFL Inf – RNFL Nasal	.853	.007	8

HTO+GS+G (LH)	Pearson Correlation	Sig. (2-tailed)	N
V2v – VP	.851	.000	21
V2v – V2d	.600	.004	21
VP – V2d	.451	.035	21
VP – V3	.483	.026	21
RNFL Sup – RNFL Inf	.861	.000	21
RNFL Sup – RNFL Nasal	.684	.001	21
RNFL Inf – RNFL Nasal	.856	.000	21

HTO (LH)	Pearson Correlation	Sig. (2-tailed)	N
V2v – VP	.823	.006	9
V2v – V3	.735	.024	9
VP – V3	.805	.009	9
VP – RNFL Temp	.672	.048	9
V2d – RNFL Sup	-0.665	.050	9

GS (LH)	Pearson Correlation	Sig. (2-tailed)	N
V2v – VP	.807	.015	8
RNFL Sup – RNFL Inf	.897	.002	8
RNFL Sup – RNFL Nasal	.759	.029	8
RNFL Inf – RNFL Nasal	.858	.006	8

G (LH)	Pearson Correlation	Sig. (2-tailed)	Spearman Correlation	Sig (2-tailed)	N
V2v – VP	.968	.012	1.000	.000	4
V2v – V2d	.991	.009	0.800	N.S.	4
VP – V2d	.968	.032	0.800	N.S.	4
RNFL Sup – RNFL Inf	.994	.006	1.000	.000	4
RNFL Sup – RNFL Nasal	.953	.047	0.800	N.S.	4
RNFL Inf –RNFL Nasal	.978	.022	0.800	N.S.	4

HTO+GS+G (RH)	Pearson Correlation	Sig. (2-tailed)	N
V1 – V2d	.434	.049	21
V2v – VP	.502	.020	21
V2v – V2d	.510	.032	21
RNFL Sup – RNFL Inf	.681	.001	21
RNFL Sup – RNFL Nasal	.488	.025	21
RNFL Inf – RNFL Nasal	.668	.001	21

HTO (RH)	Pearson Correlation	Sig. (2-tailed)	N
V2v – V2d	.785	.012	9
V3 – RNFL Sup	-0.857	.003	9

GS (RH)	Pearson Correlation	Sig. (2-tailed)	N
V1 – V2d	.878	.004	8
V2v – VP	.830	.011	8
RNFL Sup – RNFL Temp	-0.837	.010	8

The strong correlations (Pearson coefficient) found for the G group with parametric statistics mostly survive the non-parametric analysis; however, the absolute values of correlations coefficients should be taken with care when performing tests in a group with a small numbers of subjects.

G (RH)	Pearson Correlation	Sig. (2-tailed)	Spearman Correlation	Sig (2-tailed)	N
V1 – V2v	.954	.046	1.000	.000	4
VP – RNFL Sup	.995	.005	1.000	.000	4
VP – RNFL Inf	.980	.020	1.000	.000	4
RNFL Sup – RNFL Inf	.960	.040	1.000	.000	4
RNFL Inf – RNFL Temp	.969	.031	1.000	.000	4
RNFL Temp – RNFL Nasal	.990	.010	0.800	N.S.	4

Table(s) 2: Correlations between retinotopic areas and retinal nerve fiber layer of the optic nerve (RNFL); the (12) data tables above present all the statistically significant correlations found between CT of visual areas and retinal thickness.

Global measures	Pearson Correlation	Sig. (2-tailed)	Spearman Correlation	Sig (2-tailed)	N
V1 – FDT_MD_OD	-	-	-0.358	.020	42
V2d – FDT_MD_OE	.320	.039	.440	.004	42
V2d – FDT_PSD_OE	-	-	-0.367	0.017	42
FDT_MD_OE – FDT_MD_OD	.927	.000	.714	.000	42
FDT_MD_OE – FDT_PSD_OE	-0.501	.001	-0.469	.002	42
FDT_MD_OE – FDT_PSD_OD	-0.804	.000	-0.358	.020	42
FDT_MD_OD – FDT_PSD_OD	-0.835	.000	-0.481	.001	42

Table 3: Variables MD and PSD, when separated by eyes (OD and OE), did not adjust to a normal distribution, so non-parametric tests were also performed.

The following plots correspond to the correlations previously highlighted in yellow.

HTO+GS+G (LH+RH)

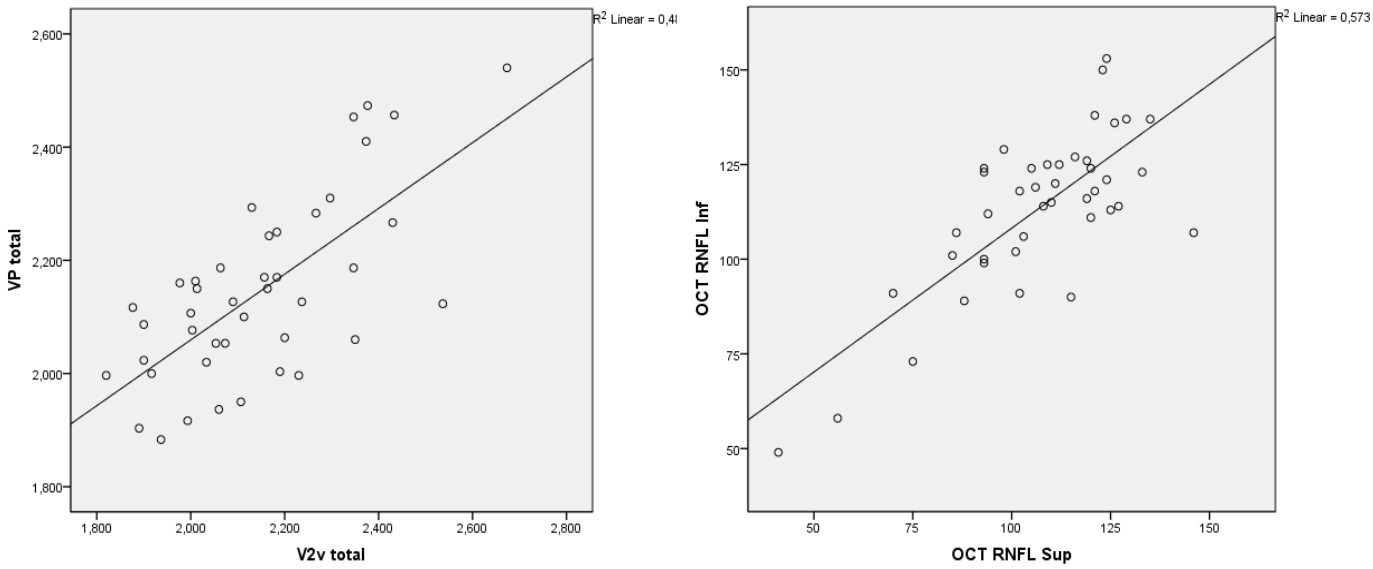

Fig. 18: V2v-VP thickness correlation is statistically significant for all groups and is one of the strongest correlations between visual areas we have found (left). Similarly, it has been found that RNFL thickness in different regions (i.e., superior, inferior and nasal) of the retina are strongly correlated (right); interestingly, the temporal region seems to be an exception for the most part.

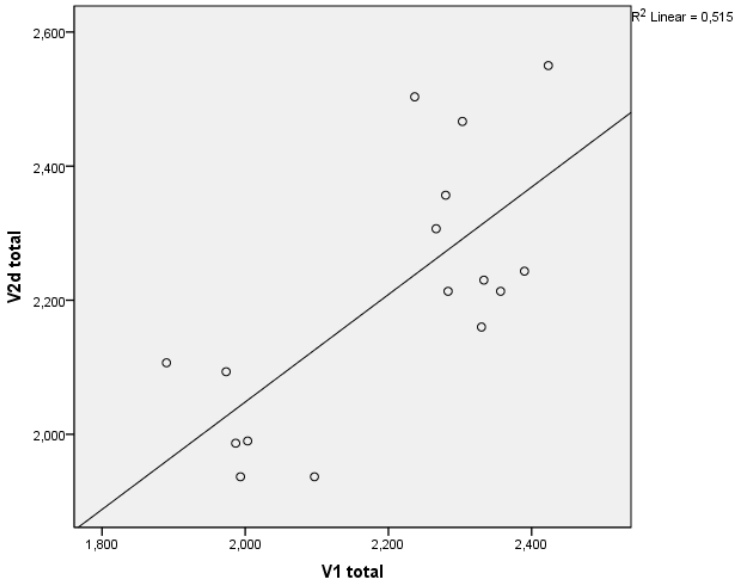

Fig. 19: A stronger correlation between V1 and V2d has been found for patients characterized as glaucoma suspects (GS). Although trends can be seen for the remaining groups, they do not reach statistical significance.

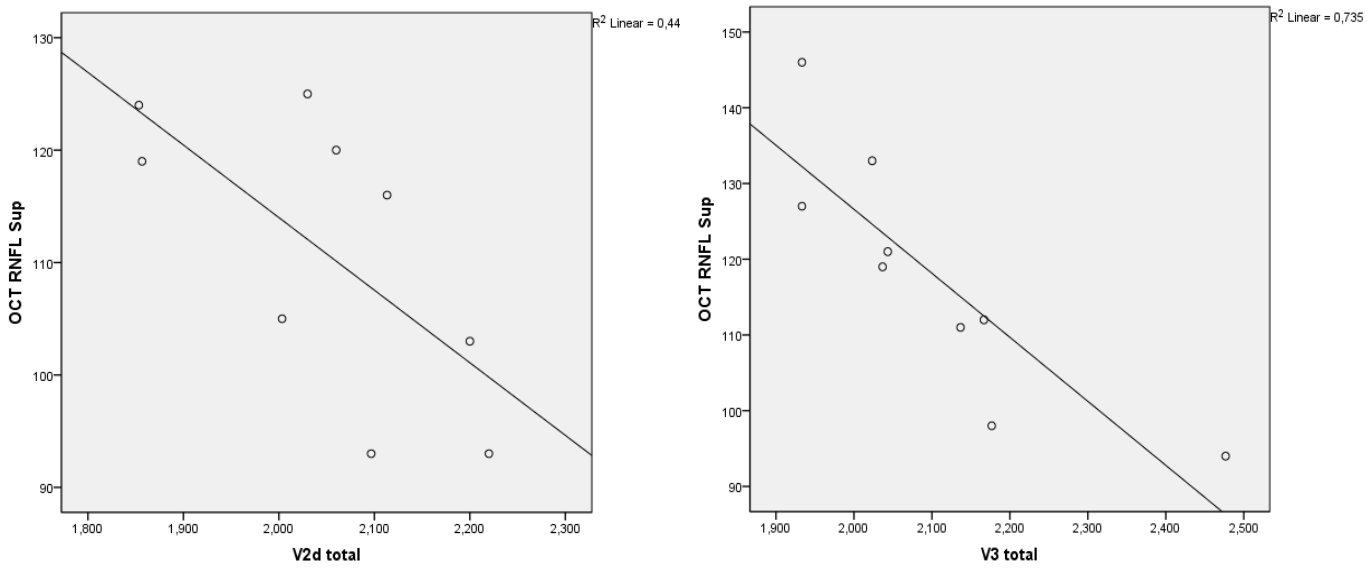

Fig. 20: A striking negative correlation has been found for HTO subjects between V2d (for LH, on the left) / V3 (for RH, on the right) and the RNFL superior region's thickness.

Correlations between thickness of retinotopic areas and retinal functional activity (FDT)

There is a recurrent hypothesis regarding the structure-function relationship in early Glaucoma (GS) where a Retinal Ganglion Cell functional reserve (or RGC redundancy) is postulated. This is consistent with the finding that even more than half of RGCs may be lost before loss in visual function is detectable by standard automated perimetry (SAP); it is assumed that there is enough redundancy of RGCs so that a subpopulation could retain normal sensitivity levels even though many other RGCs have degenerated or become dysfunctional (Quigley et al., 1992).

As previously stated, the use of FDT perimetry in a clinical setting began fairly recently, so its role in monitoring progressive field loss and the eventual correlations it has to structural loss is still being studied. In this work, we have looked for the correlations between functional sensitivity, separated either in hemifields and quadrants, and the cortical thickness in main visual areas.

Table(s) 4: Correlations between thickness of retinotopic areas and retinal functional activity (FDT); the (6) data tables below present all the statistically significant correlations found between CT of visual areas and retinal functional activity, provided by FDT.

HTO+GS+G (LH)	Pearson Correlation	Sig. (2-tailed)	N
V2d – FDT (TI_OE)	.439	.047	21

HTO (LH)	Pearson Correlation	Sig. (2-tailed)	N
V1 – FDT (LH_OE)	-0.720	.029	9
V1 – FDT (TS_OE)	-0.711	.032	9

GS (LH)	Pearson Correlation	Sig. (2-tailed)	N
V1 – FDT (NI_OE)	-0.712	.048	8
V2v – FDT (TI_OD)	-0.803	.016	8
V2d – FDT (LH_OD)	-0.769	0.026	8
V2d – FDT (TS_OD)	-0.783	0.021	8
V2d – FDT (NI_OD)	-0.766	0.027	8

G (LH)	Pearson Correlation	Sig. (2-tailed)	Spearman Correlation	Sig (2-tailed)	N
VP – FDT (TI_OE)	.963	.037	1.000	.000	4

Even though only the VP – FDT (TI_OE) correlation is significant in both parametric and non-parametric analysis, V2v and VP correlate with most FDT quadrants if we only consider the non-parametric tests.

HTO (RH)	Pearson Correlation	Sig. (2-tailed)	N
V2v – FDT (NS_OE)	.666	.050	9

GS (RH)	Pearson Correlation	Sig. (2-tailed)	N
V1 – FDT (LH_OD)	-0.760	.028	8
V2v – FDT (NI_OD)	-0.720	.044	8
V2d – FDT (RH_OD)	-0.735	0.038	8
V2d – FDT (LH_OD)	-0.817	0.013	8
V2d – FDT (NI_OD)	-0.786	0.021	8

For the right hemisphere of glaucoma patients (G), only non-parametric correlations have been found between V2d and multiple quadrants of FDT.

Finally, we have tried to assess the correlation between RNFL thickness of visual areas and central ganglion cell activity, as measured by Pattern Electroretinogram (PERG). PERG records global ganglion cell responses to a stimulus that consists in a pattern reversal checkerboard. With the available data (PERG N35-P50 and PERG P50-N95, as well as the superior, inferior, nasal and temporal RNFL thickness values), only one correlation emerged as statistically significant (for non-parametric tests):

G (LH+RH)	Pearson Correlation	Sig. (2-tailed)	Spearman Correlation	Sig. (2-tailed)	N
PERG P50-N95 – RNFL Sup	0.659	N.S. (.076)	.738	.037	8

Multivariate analysis of variance (MANOVA) and CatPCA

Due to the large number of variables we were considering and the correlations between them, we have decided to employ a more powerful statistical tool – a multivariate analysis. With MANOVA, the dependent variables are considered simultaneously, organized in a composite way and the effects associated to each variable are weighed according to the correlation that exists between them (this reduces the associated type I error) In fact, often MANOVA allows one to detect differences that would go unnoticed if only simple variate analyses (ANOVAs) were performed (Newton, 1999).

For OCT, the global analysis of variables (OCT nasal, temporal, inferior and superior) has revealed a significant difference (λ Wilks, $p<0.001$). ANOVA tests for each RNFL region revealed significant differences among groups for superior (HTO=GS≠G, $p=0.001$), inferior (HTO=GS≠G, $p<0.001$) and nasal (HTO=GS≠G, $p=0.026$) regions; for the temporal region, the difference was between the HTO and G groups ($p=0.032$).

Similarly, group differences were detected for FDT quadrants (TS, NS, NI and TI) by the MANOVA (λ Wilks, $p<0.001$); the significant differences were once again detected for the G group (HTO=GS≠G) for all quadrants. As for the cortical thickness of visual areas, no group differences have been found when evaluating the joint effects on the five regions (λ Wilks, $p>0.001$).

Since all relevant variables were quantitative, we have further studied our data with a multivariate method known as Principal Components Analysis. This technique takes a set of correlated variables and transforms it into a smaller components set – being each component (*principal component*) a linear combination of the original variables.

In order to add the 'Group variable' (HTO, GS or G), which is not quantitative, SPSS applies the *Optimal Scaling* algorithm that allows its use during the numerical analysis – the combined analytical procedure is called Categorical Principal Components Analysis (or CatPCA). This type of analysis is particularly useful to reduce the dimensionality of variables (measured in different scales); the number of components to be extracted should be enough to account for a reasonable percentage of the original data variation.

Dimension	Cronbach's Alpha	Variance Accounted For	
	Total (Eigen value)	% of Variance	Total (Eigen value)
1	.737	2.974	29.736
2	.576	2.078	20.782
Total	**.891**	5.052	50.517

Fig. 21: Total Cronbach's Alpha is based on the total Eigen value and serves as an indicator of reliability of a model. Typically a model with a Cronbach's Alpha over 0.7 is considered to be sound.

	Total (Vector Coordinates)		
	Dimension		Total
	2	1	
Group	.451	.175	.625
V1 total	.105	.014	.119
V2v total	.443	.283	.726
VP total	.199	.417	.616
V2d total	.206	.283	.488
V3 total	.038	.346	.384
OCT RNFL Sup	.552	.015	.567
OCT RNFL Inf	.610	.211	.821
OCT RNFL Temp	.184	.021	.205
OCT RNFL Nasal	.187	.314	.500
Active Total	2.974	2.078	5.052
% of Variance	29.736	20.782	50.517

	Dimension	
	1	2
Group	-.671	-.418
V1 total	-.324	.119
V2v total	-.666	.532
VP total	-.446	.646
V2d total	-.453	.532
V3 total	-.195	.588
OCT RNFL Sup	.743	.124
OCT RNFL Inf	.781	.459
OCT RNFL Temp	.429	.146
OCT RNFL Nasal	.432	.560

Fig. 22: Variance accounted for the present variables (left); individual component loadings (right). Tests were evaluated at the 0.05 significance level. Plot of the principal component loadings (below).

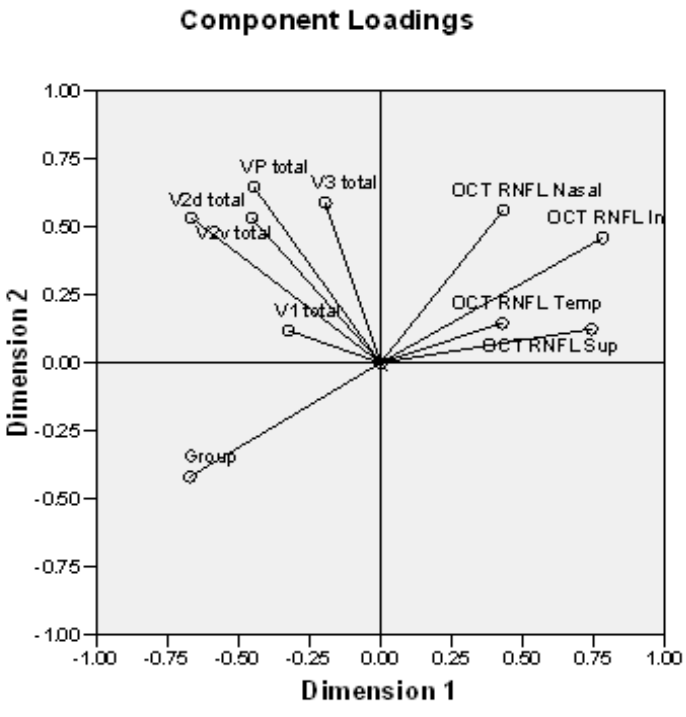

Variable Principal Normalization.

LHON (2nd part of study)

Cortical thickness of retinotopic areas

Leber hereditary optic neuropathy (LHON) is characterized by bilateral, subacute visual failure that develops during young adulthood; males are more prone (approximately four times) to develop this condition than females. These patients are usually asymptomatic until they develop visual blurring that affects the central visual field of one eye; however, similar symptoms appear in the other eye weeks later. Nevertheless, in about a quarter of the cases, visual loss is bilateral at onset. Visual acuity is severely reduced visual field testing (e.g., perimetry) shows an enlarging central or scotoma. Later, after the initial acute phase, the optic discs become atrophic. Improvements in visual acuity are rare and most of these patients will present a visual acuity of ≤20/200, which classifies them as blind. Mutations in the mitochondrial genes that encode subunits of NADH dehydrogenase, *MT-ND1*, *MT-ND2*, *MT-ND4*, *MT-ND5*, and *MT-ND6*, are known to be associated with LHON.

The table below presents all CT measurements used during this part of the study; all values are in millimeters. In total, 20 Leber's hereditary optic neuropathy patients performed the anatomical/functional MRI exams and underwent a full optic assessment (retinian and RNFL thickness of the macula and RNFL thickness of the optic nerve). In terms of CT of visual areas, there are six rows of data for each subject (ID) – foveal, intermediate and peripheral sub-regions, for both hemispheres. *Average* and *Total* values were calculated for each sub-region and visual area, respectively.

ID	Age	Group	Hemisphere	V1 avg	V1 tot.	V2v avg	V2v tot.	VP avg	VP tot.	V2d avg	V2d tot.	V3 avg	V3 tot.
3	67	LHON	LH - fovea	1,56		2,05		2,15		1,82		1,80	
3	67	LHON	LH - inter.	1,82	1,83	2,43	2,30	2,22	2,22	2,13	2,09	1,91	1,90
3	67	LHON	LH - perif.	2,10		2,41		2,29		2,31		2,00	
3	67	LHON	RH - fovea	1,88		2,10		2,17		1,99		2,16	
3	67	LHON	RH - inter.	1,91	2,08	2,48	2,56	2,38	2,24	2,10	2,14	2,37	2,18
3	67	LHON	RH - perif.	2,44		3,11		2,16		2,34		2,00	
13	20	LHON	LH - fovea	1,93		2,24		2,14		2,06		2,10	
13	20	LHON	LH - inter.	2,95	2,30	2,31	2,29	2,59	2,26	2,18	2,20	1,86	1,98
13	20	LHON	LH - perif.	2,03		2,33		2,04		2,36		1,97	
13	20	LHON	RH - fovea	2,41		2,08		2,19		1,50		2,06	
13	20	LHON	RH - inter.	2,52	2,42	2,28	2,26	2,27	2,33	2,48	2,27	2,53	2,27
13	20	LHON	RH - perif.	2,34		2,41		2,54		2,83		2,23	
17	12	LHON	LH - fovea	2,00		1,71		1,80		1,67		2,09	
17	12	LHON	LH - inter.	2,68	2,32	2,07	2,01	2,36	2,02	2,84	2,44	2,20	2,25
17	12	LHON	LH - perif.	2,27		2,26		1,91		2,81		2,45	
17	12	LHON	RH - fovea	1,65		1,47		1,83		1,92		2,01	
17	12	LHON	RH - inter.	2,58	2,13	2,30	1,99	2,12	1,99	2,67	2,38	2,33	2,20
17	12	LHON	RH - perif.	2,16		2,19		2,01		2,55		2,27	

11	20	LHON	LH - fovea	2,12		2,02		2,05		2,14		2,17	
11	20	LHON	LH - inter.	2,23	2,25	2,21	2,14	2,54	2,37	2,62	2,52	2,05	2,19
11	20	LHON	LH - perif.	2,40		2,19		2,51		2,79		2,35	
11	20	LHON	RH - fovea	2,33		2,68		1,99		2,08		2,22	
11	20	LHON	RH - inter.	2,22	2,25	2,93	2,71	2,22	2,17	2,40	2,43	2,40	2,33
11	20	LHON	RH - perif.	2,21		2,53		2,29		2,81		2,36	
8	37	LHON	LH - fovea	2,03		2,49		2,73		1,85		2,44	
8	37	LHON	LH - inter.	2,14	2,16	2,27	2,46	2,88	2,62	2,23	2,00	2,33	2,30
8	37	LHON	LH - perif.	2,32		2,61		2,25		1,92		2,14	
8	37	LHON	RH - fovea	2,18		2,26		2,15		1,46		2,07	
8	37	LHON	RH - inter.	2,35	2,21	2,22	2,22	2,23	2,35	2,47	2,19	2,26	2,18
8	37	LHON	RH - perif.	2,11		2,19		2,67		2,65		2,20	
15	17	LHON	LH - fovea	2,08		2,46		1,99		2,13		2,40	
15	17	LHON	LH - inter.	2,07	2,12	2,79	2,54	2,58	2,32	2,40	2,31	2,45	2,32
15	17	LHON	LH - perif.	2,21		2,36		2,40		2,40		2,11	
15	17	LHON	RH - fovea	2,22		2,36		2,41		1,93		2,21	
15	17	LHON	RH - inter.	2,13	2,36	2,97	2,74	2,76	2,53	2,59	2,27	2,22	2,24
15	17	LHON	RH - perif.	2,72		2,90		2,42		2,29		2,28	
7	38	LHON	LH - fovea	1,97		2,42		2,48		1,83		2,27	
7	38	LHON	LH - inter.	1,73	1,87	2,17	2,14	2,63	2,45	1,92	1,85	2,28	2,19
7	38	LHON	LH - perif.	1,90		1,82		2,23		1,79		2,03	
7	38	LHON	RH - fovea	2,34		2,61		1,88		2,12		1,98	
7	38	LHON	RH - inter.	2,07	2,21	2,95	2,73	2,16	2,06	1,80	1,96	1,76	1,85
7	38	LHON	RH - perif.	2,22		2,64		2,13		1,95		1,81	
9	35	LHON	LH - fovea	2,13		3,03		2,76		2,07		2,24	
9	35	LHON	LH - inter.	2,65	2,44	3,00	2,88	3,01	2,79	2,21	2,13	2,64	2,38
9	35	LHON	LH - perif.	2,53		2,61		2,61		2,11		2,26	
9	35	LHON	RH - fovea	2,21		2,32		2,28		2,18		2,05	
9	35	LHON	RH - inter.	2,41	2,30	2,51	2,40	2,71	2,67	2,18	2,33	2,36	2,23
9	35	LHON	RH - perif.	2,27		2,36		3,01		2,62		2,27	
14	17	LHON	LH - fovea	1,99		2,30		3,07		2,61		2,41	
14	17	LHON	LH - inter.	2,30	2,17	2,92	2,56	2,63	2,83	2,06	2,24	2,31	2,38
14	17	LHON	LH - perif.	2,21		2,45		2,79		2,05		2,42	
14	17	LHON	RH - fovea	2,43		2,12		2,13		2,04		2,67	
14	17	LHON	RH - inter.	2,63	2,49	3,06	2,79	2,65	2,49	2,35	2,51	2,44	2,55
14	17	LHON	RH - perif.	2,40		3,18		2,69		3,15		2,55	
20	7	LHON	LH - fovea	2,41		1,99		2,22		2,20		2,53	
20	7	LHON	LH - inter.	1,95	2,17	2,69	2,50	2,63	2,65	2,35	2,43	2,34	2,54
20	7	LHON	LH - perif.	2,14		2,83		3,11		2,74		2,75	
20	7	LHON	RH - fovea	2,52		2,65		2,57		2,38		2,70	
20	7	LHON	RH - inter.	3,30	2,74	2,89	3,16	2,75	2,70	3,02	2,75	3,04	2,78
20	7	LHON	RH - perif.	2,41		3,94		2,79		2,85		2,61	
6	39	LHON	LH - fovea	1,68		2,44		2,18		2,18		2,95	
6	39	LHON	LH - inter.	3,05	2,33	3,00	2,66	2,84	2,85	2,35	2,31	3,00	2,82
6	39	LHON	LH - perif.	2,27		2,53		3,53		2,39		2,51	
6	39	LHON	RH - fovea	2,07		2,24		2,37		2,05		2,17	
6	39	LHON	RH - inter.	3,00	2,49	3,46	2,89	3,23	2,69	2,84	2,56	2,48	2,37
6	39	LHON	RH - perif.	2,40		2,97		2,48		2,78		2,46	
5	41	LHON	LH - fovea	2,03		2,62		1,92		2,37		1,93	
5	41	LHON	LH - inter.	2,73	2,49	2,46	2,60	2,21	2,16	2,41	2,29	2,83	2,38
5	41	LHON	LH - perif.	2,71		2,71		2,34		2,09		2,39	
5	41	LHON	RH - fovea	2,16		2,31		2,49		1,77		2,30	

5	41	LHON	RH - inter.	2,98	2,62	2,94	2,69	2,70	2,62	2,11	2,05	2,57	2,34
5	41	LHON	RH - perif.	2,71		2,81		2,66		2,28		2,16	
2	44	LHON	LH - fovea	1,81		2,42		2,35		2,61		2,40	
2	44	LHON	LH - inter.	2,46	2,31	3,06	2,65	2,80	2,68	2,97	2,82	2,87	2,50
2	44	LHON	LH - perif.	2,65		2,46		2,90		2,88		2,22	
2	44	LHON	RH - fovea	2,29		3,03		2,61		1,79		2,42	
2	44	LHON	RH - inter.	3,15	2,71	3,63	3,37	3,47	3,02	2,77	2,15	2,70	2,58
2	44	LHON	RH - perif.	2,69		3,46		2,97		1,90		2,62	
1	45	LHON	LH - fovea	2,16		1,86		2,33		2,43		1,91	
1	45	LHON	LH - inter.	2,52	2,47	2,89	2,47	2,82	2,57	2,76	2,52	2,45	2,15
1	45	LHON	LH - perif.	2,73		2,66		2,56		2,38		2,10	
1	45	LHON	RH - fovea	2,07		2,48		2,42		2,09		2,44	
1	45	LHON	RH - inter.	2,96	2,45	3,23	2,97	2,66	2,50	2,46	2,85	2,67	2,58
1	45	LHON	RH - perif.	2,33		3,19		2,41		3,99		2,63	
19	8	LHON	LH - fovea	2,16		3,41		2,63		2,70		2,86	
19	8	LHON	LH - inter.	1,90	2,01	3,87	3,69	2,19	2,61	2,42	2,76	2,64	2,77
19	8	LHON	LH - perif.	1,97		3,79		3,01		3,15		2,80	
19	8	LHON	RH - fovea	2,71		3,53		3,23		1,87		2,83	
19	8	LHON	RH - inter.	2,88	2,58	3,65	3,39	3,32	3,04	2,60	2,49	3,00	2,83
19	8	LHON	RH - perif.	2,15		2,99		2,58		2,99		2,65	
12	15	LHON	LH - fovea	2,15		2,77		2,14		2,37		2,65	
12	15	LHON	LH - inter.	2,64	2,35	2,92	3,06	3,19	2,62	2,51	2,71	3,15	2,88
12	15	LHON	LH - perif.	2,26		3,48		2,53		3,26		2,84	
12	15	LHON	RH - fovea	1,66		2,74		2,61		1,57		2,09	
12	15	LHON	RH - inter.	2,85	2,29	2,57	2,79	3,56	3,07	2,17	2,11	2,13	2,22
12	15	LHON	RH - perif.	2,36		3,07		3,04		2,60		2,44	
18	18	LHON	LH - fovea	1,85		2,12		2,24		1,92		1,94	
18	18	LHON	LH - inter.	2,33	2,04	2,35	2,21	1,90	2,10	2,55	2,29	2,38	2,19
18	18	LHON	LH - perif.	1,94		2,17		2,15		2,39		2,24	
18	18	LHON	RH - fovea	1,76		2,18		2,49		1,80		1,94	
18	18	LHON	RH - inter.	2,36	2,10	3,22	2,54	2,54	2,35	2,37	2,31	2,22	2,15
18	18	LHON	RH - perif.	2,17		2,23		2,01		2,76		2,28	
22	23	LHON	LH - fovea	2,28		2,33		2,42		2,36		2,55	
22	23	LHON	LH - inter.	2,70	2,46	2,79	2,67	2,72	2,53	2,18	2,48	2,82	2,76
22	23	LHON	LH - perif.	2,40		2,88		2,45		2,89		2,90	
22	23	LHON	RH - fovea	2,51		2,75		2,60		2,24		2,45	
22	23	LHON	RH - inter.	3,21	3,03	3,19	3,19	3,48	3,04	3,05	2,70	3,01	2,84
22	23	LHON	RH - perif.	3,36		3,63		3,05		2,80		3,05	
16	25	LHON	LH - fovea	2,00		2,34		2,15		1,85		2,08	
16	25	LHON	LH - inter.	2,31	2,24	1,82	2,03	2,05	2,36	2,18	2,09	2,34	2,19
16	25	LHON	LH - perif.	2,40		1,93		2,87		2,25		2,15	
16	25	LHON	RH - fovea	2,02		2,78		2,26		1,76		2,25	
16	25	LHON	RH - inter.	2,28	2,17	1,99	2,53	2,40	2,31	2,52	2,37	2,03	2,13
16	25	LHON	RH - perif.	2,22		2,81		2,28		2,83		2,12	
10	29	LHON	LH - fovea	1,91		2,06		1,78		1,89		2,22	
10	29	LHON	LH - inter.	2,03	2,04	2,19	2,17	2,78	2,48	2,39	2,17	2,33	2,26
10	29	LHON	LH - perif.	2,18		2,26		2,88		2,22		2,23	
10	29	LHON	RH - fovea	2,06		1,81		2,74		2,24		2,02	
10	29	LHON	RH - inter.	2,37	2,24	2,49	2,36	2,88	2,72	2,37	2,33	2,14	2,17
10	29	LHON	RH - perif.	2,28		2,79		2,53		2,39		2,34	

Table 5: Values of cortical thickness for individual visual areas of 20 LHON subjects.

Correlations between thickness of retinotopic areas and retinal nerve fiber layer of the optic nerve (RNFL) and macular regions

The correlations between the cortical thickness of visual areas and the RNFL of the optic nerve were primarily obtained with parametric statistics (Pearson Correlation coefficient). The analyses were performed using all data (CT from both hemispheres) and, when appropriate, for each hemisphere. All variables follow a normal distribution (Kolmogorov-Smirnov test, $p>0.01$).

LH+RH (N=40)		V2v Total	VP Total	V2d Total	V3 Total
V1 Total	Pearson Correlation	,521	,509	,406	,554
	Sig. (2-tailed)	,001	,001	,009	,000
V2v Total	Pearson Correlation		,614	,454	,691
	Sig. (2-tailed)		,000	,003	,000
VP Total	Pearson Correlation				,599
	Sig. (2-tailed)			N.S.	,000
V2d Total	Pearson Correlation				,627
	Sig. (2-tailed)				,000

Table 6: Correlations between cortical thickness of individual visual areas of 20 LHON subjects; only VP – V2d did not reach statistical significance.

To rule out the possibility of these correlations being heavily age-dependent, we have divided our data set into two groups, by choosing a threshold age of 21.

Age <= 21 (N=18)		V2v Total	VP Total	V2d Total	V3 Total
V1 Total	Pearson Correlation				
	Sig. (2-tailed)	N.S.	N.S.	N.S.	N.S.
V2v Total	Pearson Correlation		,687	,564	,800
	Sig. (2-tailed)		,002	,015	,000
VP Total	Pearson Correlation				,550
	Sig. (2-tailed)			N.S.	,018
V2d Total	Pearson Correlation				,797
	Sig. (2-tailed)				,000

Table 7: Correlations between cortical thickness of individual visual areas of LHON subjects younger than 21; other than VP – V2d, none of V1 correlations reached statistical significance (above). However, for subjects older than 21, the correlations between V1 and all other visual areas reappear (below).

Age > 21 (N=22)		V2v Total	VP Total	V2d Total	V3 Total
V1 Total	Pearson Correlation	,776	,625	,508	,677
	Sig. (2-tailed)	,000	,002	,016	,001
V2v Total	Pearson Correlation		,548		,581
	Sig. (2-tailed)		,008	N.S.	,005
VP Total	Pearson Correlation				,700
	Sig. (2-tailed)			N.S.	,000
V2d Total	Pearson Correlation				,540
	Sig. (2-tailed)				,010

Visual areas – RNFL optic nerve	Pearson Correlation	Sig. (2-tailed)	N
V1 – RNFL_NI_OE	.371	.048	38
V2v – RNFL_NI_OE	.436	.006	38
VP – RNFL_NI_OE	.357	.028	38
VP – RNFL_NI_OD	.498	.001	38

Table 8: Correlations between cortical thickness of individual visual areas of LHON subjects and RNFL thickness in the optic nerve (average values by quadrants).

RNFL optic nerve	Pearson Correlation	Sig. (2-tailed)	N
TS_OE – TS_OD	.586	.000	38
TS_OE – TI_OE	.605	.000	38
TS_OD – TI_OD	.552	.000	38
TI_OE – TI_OD	.498	.001	38

Table 9: Correlations between RNFL thickness of different quadrants in the optic nerve. Despite having found several correlations among RNFL thickness of different optic nerve regions, the strongest ones were interestingly between temporal regions (different regions in the same eye or same region in different eyes).

As for the last structural analysis, we have decided to look into possible differences in retinocortical correlations according to eccentricity. For this purpose, OCT thickness values of the macular retina were divided into three rings (1 – foveal region, 2 – intermediate region, 3 – peripheral region); Cortical thickness was sampled similarly, providing an average CT value for foveal, intermediate and peripheral sub-regions for each visual area.

Eccentricity Visual areas – macular OCT	Pearson Correlation	Sig. (2-tailed)	N
V1 Int – Ring 2_OE	-0.462	.004	38
V1 Int – Ring 2_OD	-0.463	.003	40
V1 Int – Ring 3_OE	-0.474	.003	38
V1 Int – Ring 3_OD	-0.493	.001	40
V2v Per – Ring 2_OE	-0.483	.002	38
V2v Per – Ring 3_OE	-0.471	.003	38
V2d Int – Ring 2_OE	-0.450	.005	38
V2d Int – Ring 2_OD	-0.360	.023	40
V2d Int – Ring 3_OE	-0.446	.005	38
V2d Per – Ring 3_OE	-0.376	.020	38
V3 Per – Ring 3_OE	-0.419	.009	38

Table 10: Correlations between thickness of individual visual areas (by eccentricity of VF representation) and thickness of the macular retina (by eccentricity rings).

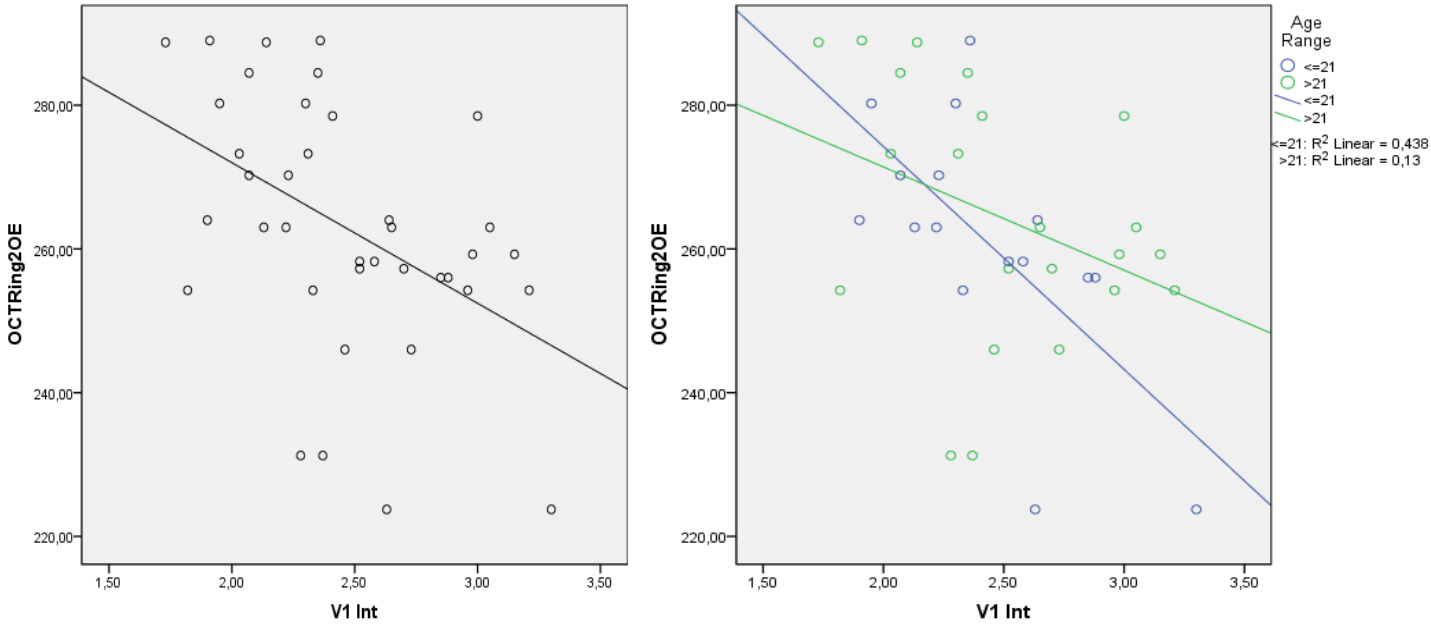

Fig. 23: Correlations between V1 (intermediate sub-region) thickness and average thickness of the *intermediate ring* (Ring 2) of the macular retina; all LHON subjects (left) and age-grouped (right) where blue dots represent younger subjects (<21) and green dots represent older subjects (>21). The correlation results were virtually identical whether we considered OCT values from the left (OE) or the right (OD) eye.

Correlations between thickness of retinotopic areas and sensory performance (SAP)

For the functional global measures, MD(dB) and LV(dB), there was a statistically significant correlation between them (Pearson coefficient of 0.581, $p<0.001$). As LV did not follow a normal distribution, we used a non-parametric test that confirmed the correlation (Spearman coefficient of 0.518, $p=0.001$); data from both hemispheres were included. Additionally, LV correlated with all macular regions of both eyes (i.e., with its thickness values); Spearman coefficient ranged from 0.363 (Nasal OE) to 0.527 (Temporal OE), $p<0.01$, $n=39$.

Leber (LH+RH) Visual areas – SAP (dB)	Pearson Correlation	Sig. (2-tailed)	N
V1 – TS_OD	.363	.021	40
VP – TI_OE	.436	.006	40
V3 – TS_OD	.414	.008	40
V3 – NI_OD	.335	.034	40

Leber (LH) Visual areas – SAP (dB)	Pearson Correlation	Sig. (2-tailed)	N
VP – TI_OE	.466	.044	20
V3 – TS_OD	.498	.025	20
V3 – NI_OD	.508	.022	20
V3 – TI_OE	.505	.028	20

Leber (RH) Visual areas – SAP (dB)	Pearson Correlation	Sig. (2-tailed)	N
V1 – TS_OD	.466	.038	20

Table(s) 11: Correlations between thickness of retinotopic areas and sensory performance (SAP); the (3) data tables above present all the statistically significant correlations found between CT of visual areas and sensory performance, provided by SAP. All variables follow a normal distribution (Kolmogorov-Smirnov test, $p>0.01$).

Once again, it is the temporal region that seems to be more closely correlated with structural alterations at the cortical level; the most significant correlations were found predominantly between the functional activity of the retinal temporal region and the extrastriate areas of the left hemisphere.

When analyzing solely the functional measures, the results for each region (retinal quadrant) indicate a strong correlation among all regions.

CatPCA and FA (factor analysis)

Similarly to what we have done in the first part of this study, we analyzed our data with a multivariate method known as Principal Components Analysis, as all relevant variables were quantitative. Instead of a 'Group' variable, we wanted to explore the influence of the subjects' age (age range – two groups, threshold age of 21) on both cortical and macular retina thickness. This type of analysis is particularly useful to reduce the dimensionality of variables (measured in different scales) and reveals trends in dependency between different sets of variables.

Dimension	Cronbach's Alpha	Variance Accounted For
	Total (Eigen value)	Total (Eigen value)
1	.893	5.852
2	.667	2.628
Total	**.950**	8.480

Fig. 24: Total Cronbach's Alpha is based on the total Eigen value and serves as an indicator of reliability of a model. Typically a model with a Cronbach's Alpha over 0.7 is considered to be sound.

	Total (Vector Coordinates)		
	Dimension		Total
	2	1	2
Age Range	.064	.078	.142
V1 Total	.161	.425	.586
V2v Total	.239	.425	.665
VP Total	.239	.247	.485
V2d Total	.016	.487	.503
V3 Total	.238	.552	.790
QTSdBOE	.671	.114	.785
QTSdBOD	.648	.000	.648
QNSdBOE	.518	.039	.557
QNSdBOD	.597	.008	.605
QNIdBOE	.547	.108	.655
QNIdBOD	.597	.002	.600
QTIdBOE	.655	.083	.738
QTIdBOD	.661	.059	.720
ctive Total	5.852	2.628	8.480

	Dimension	
	1	2
Age Range	.253	-.280
V1 Total	.401	.652
V2v Total	.489	.652
VP Total	.489	.497
V2d Total	.127	.698
V3 Total	.488	.743
QTSdBOE	.819	-.338
QTSdBOD	.805	-.004
QNSdBOE	.719	-.198
QNSdBOD	.773	-.090
QNIdBOE	.740	-.329
QNIdBOD	.773	-.049
QTIdBOE	.810	-.288
QTIdBOD	.813	-.242

Fig. 25: Variance accounted for the present variables (left); individual component loadings (right). Tests were evaluated at the 0.05 significance level. Plot of the principal component loadings (below).

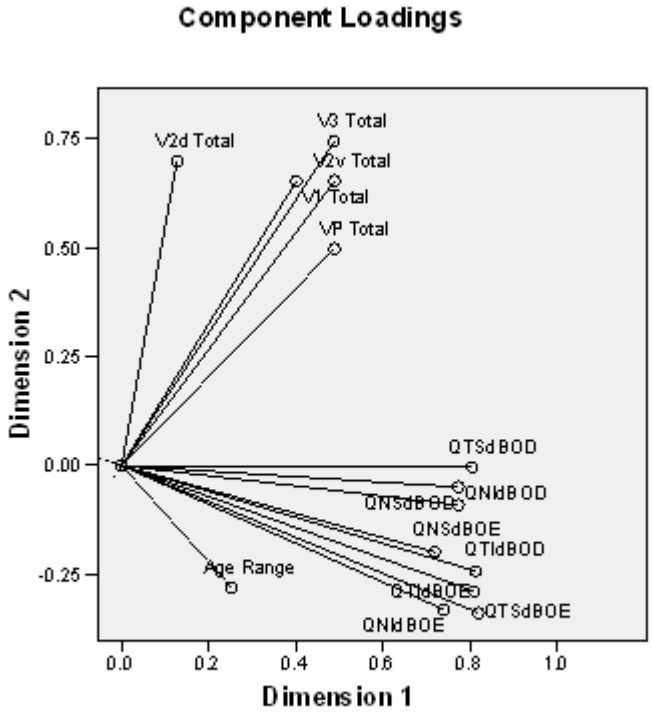

Variable Principal Normalization.

To confirm the results provided by the CatPCA, we further used a multivariate tool that allows the integration of the age data as a numerical variable (instead of a category, with only two values – '>21' or '<21'. Therefore, the subjects age will be looked at as a factor that may be influencing the other variables; therefore its name, factor analysis.

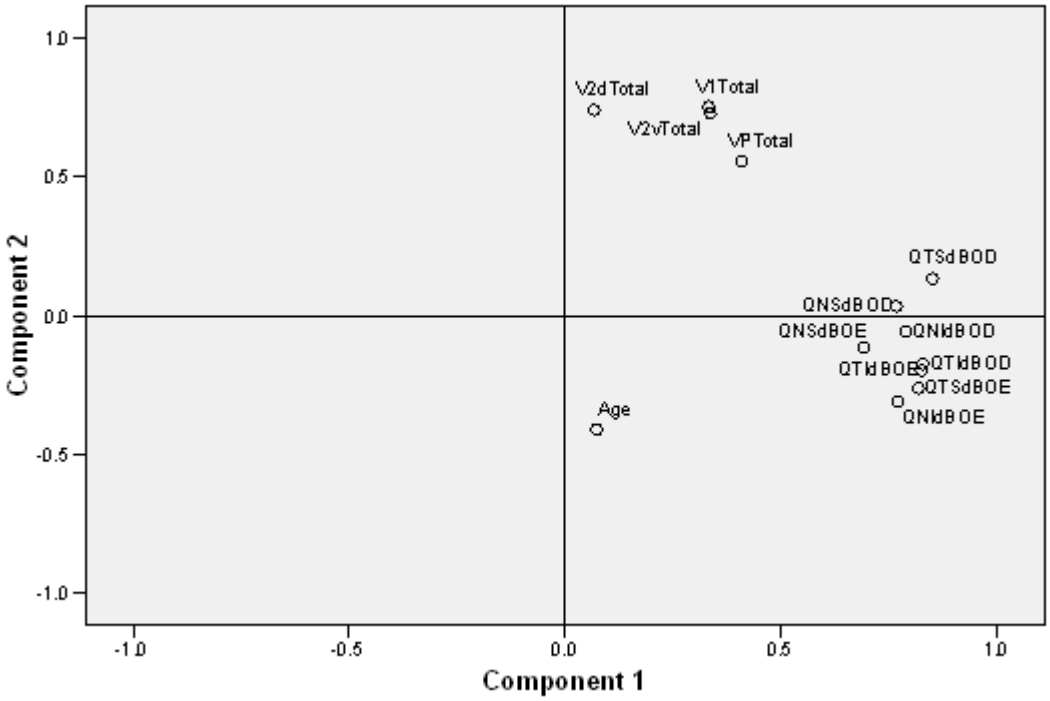

Chapter 4

Discussion

In this study, we have identified several particular traits of cortical involvement in progressive optic neuropathies. For our glaucoma patients (HTO, GS, G), we have not found evidence of any relevant cortical degeneration throughout disease progression that could account for visual loss; on the contrary, in some cases higher RGC's loss (and consequently retinal thinning) and diminished functional activity (provided by FDT), correlates with an increase in cortical thickness in certain visual areas (namely, V1 and V2d). However, for the Leber's neuropathy group, we have came across different findings. First, although CT of different visual areas was relatively well correlated, we have found that the V1 from younger subjects (<21) did not present the same structural behavior. Furthermore, we encountered a significant correlation between the RNFL thinning in the optic nerve and the reduction in cortical thickness of visual areas (mainly ventral, V2v and VP). Surprisingly, we could not finding similar correlations between the macular retina and the cortex; furthermore, when we looked for these effects in terms of eccentricity, we found a negative correlation for some sub-regions of the visual areas and the *macular rings* from which they partially received their visual input from, as if some sort of structural plasticity was going on.

Glaucoma

The V2v-VP thickness correlation is statistically significant for all groups and it is one of the strongest correlations between visual areas we have found (Table 2). This does not appear to be surprising as these areas are contiguously located in the ventral part of the visual cortex and have a strong functional connection (they encode the same quadrant of the lower visual field). Similarly, it has been found that RNFL thickness in different regions (i.e., superior, inferior and nasal) of the retina are strongly correlated; interestingly, the temporal region seems to be an exception for the most part. The particular behavior of this region is consistent with our previous reports in normal subjects and patients (Silva et al., 2008; Mendes et al., 2005).

A striking negative correlation has been found for HTO subjects between V2d (for LH, on the left) / V3 (for RH, on the right) and the RNFL superior region's thickness (Fig. 20). As V2d and V3 are both dorsal visual regions that are encoding the inferior visual field (which is represented on the superior part of the retina), this could be due to a direct effect of a localized retinal degeneration. In this way, the observed cortical behavior could be interpreted as a compensatory plasticity mechanism that is occurring early on in the degenerative process. This might also help explain some of the surprising negative structure-function correlations (FDT and V2d in GS and V1 in HTO).

When we further analyzed our data in search for a link between the retinal structure and the electrophysiological parameters (we have considered both PERG N35-P50 and PERG P50-N95, as well as the superior, inferior, nasal and temporal RNFL thickness values), we found that, for the advanced glaucoma group (G), the RNFL thickness of the superior region is correlated with the PERG- P50-N95 signals. Despite similar trend have been observed for other RNFL regions, this was the only correlation that emerged as statistically significant (non-parametric tests).

Lastly, we have subjected our data to multivariate analyses techniques, MANOVA and CatPCA. In terms of RNFL OCT, the global analysis of variables (nasal, temporal, inferior and superior) has revealed a significant difference (λ Wilks, $p<0.001$). ANOVA tests for each RNFL region revealed significant differences among groups for superior (HTO=GS≠G, $p=0.001$), inferior (HTO=GS≠G, $p<0.001$) and nasal (HTO=GS≠G, $p=0.026$) regions; for the temporal region, instead, we found differences between the HTO and G groups ($p=0.032$). One possible explanation for this difference could be an early on degeneration of the RNFL temporal region.

Similarly, group differences were detected for FDT quadrants (TS, NS, NI and TI) by the MANOVA (λ Wilks, $p<0.001$); the significant differences were once again detected for the G group (HTO=GS≠G) for all quadrants. As for the cortical thickness of visual areas, no group differences have been found when evaluating the joint effects on the five regions (λ Wilks, $p>0.001$). This corroborates the initial findings of a minimal or null CT correlation with the progression of this visual disorder.

The plot of the obtained component loadings (Fig. 22) provides a very straightforward, visual representation of these results. The RNFL thickness vectors for each region are *pointing* in the opposite direction of the *Group* variable, which implies that they are inversely related; the thickness of visual areas, however, is clearly more independent from the *Group*, as evidenced by the vectors' orthogonality.

LHON – Leber Neuropathy

Leber's hereditary optic neuropathy (LHON) is a maternally inherited mitochondrial disorder characterized by bilateral loss of central vision, most frequently found in young adult males. As it becomes clear from our initial structural analysis (Table 6), cortical thickness of the visual areas are highly correlated among each other; but this alone would not suffice to suggest that the patients present widespread anatomical alterations throughout the visual cortex. To rule out the possibility of these correlations being heavily age-dependent, we have divided our data set into two groups, by choosing a threshold age of 21. This has revealed that, although strong correlations between V1 and all extrastriate areas remain significant for the group of older subjects

(>21), they disappear for the subjects that are under 21 years of age (Table 7). From these observations, we may hypothesize that the extrastriate areas only become structurally affected in later stages of disease, while V1, as the primary area receiving visual input, follows the degenerative path at an earlier stage when the retina and the optic nerve has not yet been severely affected. This might explain the early decorrelation pattern and later association, as damage becomes widespread in the visual system.

In terms of correlations between cortical thickness of individual visual areas of LHON subjects and RNFL thickness in the optic nerve (average values by quadrants), we have found them to be significant for V1, V2v and VP (interestingly always with the nasal-inferior region of the RNFL). This suggests that the ventral visual areas of the cortex are being affected first by alterations at the retina level (Table 8). However, the retinal impact in the cortex could not be associated to the degeneration of the macular region, since no positive correlations between macular retina thickness (OCT) and cortical thickness of visual areas have been found.

When looking only at the retinal data, strong correlations were found between thickness of all regions of the macular retina, which is in agreement with a progressive degeneration that does not preferentially develop in any macular region.

In the following structural analysis, we have decided to look into possible differences in retinocortical correlations according to eccentricity. The results revealed a surprising negative correlation for the average thickness of the macular eccentricity rings and the CT of visual areas. These effects were particularly relevant for the intermediate (V1_Int and V2d_Int) and peripheral (V2d_Per and V3_Per) sub-regions of the dorsal visual areas. As stated above, such correlations may suggest a sort of structural plasticity which may occur when most patients are mostly carriers of a disease mutation (11778 G to A mtDNA point mutation as investigated by standard PCR and automatic sequencing methods).

As for the structure-function (CT – SAP) correlations in LHON subjects, it is the temporal region that seems to be more closely correlated with structural alterations at the cortical level; the most significant correlations were found predominantly between the sensory performance corresponding to the retinal temporal region and extrastriate areas (VP and V3) of the left hemisphere.

When analyzing solely the functional measures, the results for each region (retinal quadrant) indicate a strong correlation among all regions.

Finally, the multivariate approach revealed the partial dependence between the functional activity in the retina and cortical thickness (particularly clear for VP), while age appeared as a factor that is negatively related to the CT of visual areas; this effect is more clear with the FA than with the CatPCA, where age range (only two classes) is considered.

We conclude that the pattern of visual loss is different in the two studied visual conditions, glaucoma and Leber neuropathy. In the latter we found evidence for a correlation between cortical thickness and sensory performance and structural evidence for compensatory plasticity. Such plasticity seems to be weaker in glaucoma, which is consistent with the idea that brains of subjects form older populations are less prone to plastic changes. Future studies should further explore in larger samples of subjects the surprising correlational patterns we have found in this study.

References

Braddick, O. J. and O'Brian, J. D. *(*2001). Brain areas sensitive to visual motion. *Perception,* 30, 61-72.

Brindley, G. S., and Lewin, W. S. (1968). The sensations produced by electrical stimulation of the visual cortex. *J. Physio*. 196, 479-493.

Dacey, D.M. (1993). Morphology of a small-field bistratified ganglion cell type in the macaque and human retina. *Visual Neuroscience*, 10(6), 1081-98.

DeYoe, E.A., Carman, G.J., Bandettini, P., Glickman, S., Wieser, J., Cox, R., Miller, D., and Neitz, J. (1996). Mapping striate and extrastriate visual areas in human cerebral cortex. *PNAS*, 93, 2382-2386.

Dong, D.W. and Atick, J.J. (1995). Temporal Decorrelation: A Theory of Lagged and Nonlagged Responses in the Lateral Geniculate Nucleus. Network, 6(2), 159-178.

Engel, S.A., Glover, G.H., and Wandell, B.A. (1997). Retinotopic organization in human visual cortex and the spatial precision of functional MRI. *Cereb. Cortex*, 7, 181-192.

Farivar, R. (2009). Dorsal-ventral integration in object recognition. *Brain Research Reviews,* 61(2), 144-153.

Gazzaniga, M.S. (2004). The Cognitive Neurosciences III. 3rd ed. MIT Press.

Hardan, A.Y.; Muddasani, S.; Vemulapalli, M.; Keshavan, M.S. and Minshew, N.J. (2006). An MRI Study of Increased Cortical Thickness in Autism. *Amer. J. Psychiatry*, 163(7), 1290-1292.

Hee, M.R., Swanson, E.A., et al., (1995). Optical coherence tomography of the human retina. Arch Ophthalmology, 113, 325-332.

Holmes, G. (1918). Disturbances of vision by cerebral lesions. Bre. J. Opthal. 2, 353-384.

Hubel, D.H. (1963). The visual cortex of the brain. *Scientific American, 209*(5), 54-62.

Johnson, C.A. and Samuels, S.J. (1997). Screening for glaucomatous visual field loss with frequency-doubling perimetry. Invest Ophthalmol Vis Sci, 38, 413-25.

Jones, S.E., Buchbinder, B.R. and Aharon, I. (2000). Three-dimensional mapping of cortical thickness using Laplace's equation. *Human Brain Mapping*, 11, 12–32.

Kandel, E.R., Schwartz, J.H. and Jessel, T.M. (2000). Principles of Neural Science. 4th ed. McGraw-Hill Medical.

Kelly, D.H. (1966). Frequency doubling in visual responses. J Opt Soc Am, 56, 1628-33.

Kelly, D.H. (1981). Nonlinear visual responses to flickering sinusoidal gratings. J Opt Soc Am, 71, 1051-1055.

Kolb, H. (2003). How the Retina Works. *American Scientist*, 91.

Land, M. F. and Fernald, R. D. (1992). The Evolution of Eyes. *Annual Review of Neuroscience*, 15, 1-29.

Livingstone, M. & Hubel, D.H. (1988). Segregation of form, color, movement, and depth: anatomy, physiology, and perception. *Science*, 240, 740-749.

Maddess, T. and Henry, G.H. (1992). Performance of nonlinear visual units in ocular hypertension and glaucoma. Clin Vision Sci., 7, 371-83.

Mendes, M., Silva, F., Simões, L., Jorge, M., Saraiva, J. and Castelo-Branco, M. (2005). Visual magnocellular and structure from motion perceptual deficits in a neurodevelopmental model of dorsal stream function. *Brain Res Cogn Brain Res*, 25(3), 788-98.

Minkowski, M. (1920). *Arch. Neurol. Psychiar*, 6, 201.

Mishkin, M. and Ungerleider, L.G. (1982). Contribution of striate inputs to the visuospatial functions of parieto-preoccipital cortex in monkeys. *Behav Brain Res*, 6(1), 57-77.

Munk, H. (1881). On the functions of the cortex. In The Cerebral Cortex, G. Von Bonin, eds. (Springfield, Illinois), pp. 97–117.

Newton, R.R. and Rudestam, K.F. (1999). *Your statistical consultant. Answers to your data analysis questions*. Sage publications, Inc. Thousand Oaks.

Nicholls, J.G., Martin, A.R., Wallace, B.G. and Fuchs, P.A. (2001). From Neuron to Brain. Sunderland, Mass: Sinauer Associates.

Ogawa, S. and Lee, T.M. (1990). Magnetic resonance imaging of blood vessels at high fields: In vivo and in vitro measurements and image simulation. *Magn. Reson. Med.*, 16, 9-18.

Penfield, W. and Jasper, H. (1954). Epilepsy and the Functional Anatomy of the Human Brain. London: Churchill.

Penfield, W. and Rasmussen, T. (1952). The Cerebral Cortex of Man. New York: Macmillan.

Porciatti, V., Ventura, L.M., Sorokac, N., De Los Santos, R., Feuer, W.J. (2006). *Invest Ophthalmol Vis Sci.*, 47(9), 3904-3911.

Punjabi, O.S., Lin, S.C. and Stamper, R.L. (2006). Advances in Mapping the Glaucomatous Visual Field: From Confrontation to Multifocal Visual Evoked Potentials. *The Internet Journal of Ophthalmology and Visual Science*, 4(1).

Qiu, F.T. and Heydt, R. (2005). Figure and Ground in the Visual Cortex: V2 Combines Stereoscopic Cues with Gestalt Rules. *Neuron*, 47, 155-166.

Quigley, H.A., Katz, J., Derick, R.J., et al. (1992). An evaluation of optic disc and nerve fiber layer examinations in monitoring progression of early glaucoma damage. *Ophthalmology*, 99, 19–28.

Rajimehr, R. and Tootell, R.B. (2009). Does retinotopy influence cortical folding in primate visual cortex? *J Neuroscience*, 29(36), 11149-52.

Rosa, M.G. (2002). Visual maps in the adult primate cerebral cortex: some implications for brain development and evolution. *Braz J Med Biol Res,* 35(12), 1485-1498.

Salat, D.H., Buckner, R.L., Snyder, A.Z., Greve, D.N., Desikan, S.R., Busa, E., Morris, J.C., Dale, A.M. and Fischl, B. (2004). Thinning of the Cerebral Cortex in Aging. *Cerebral Cortex*, 14, 721-730.

Sereno, M. I., Dale, A. M., Repapas, J. B., Kwong, K. K., Belliveau, J. W., Brady, T. J., Rosen, B. R. and Tootell, R. B. (1995). Borders of Multiple Visual Areas in Humans revealed by Functional Magnetic Resonance Imaging. *Science*, 268, 889-893.

Silva, M.F., Maia-Lopes, S., Mateus, C., Guerreiro, M., Sampaio, J., Faria, P. and Castelo-Branco, M. (2008). Retinal and cortical patterns of spatial anisotropy in contrast sensitivity tasks. *Vision Res*, 48(1), 127-35.

Talbot, S.A. (1940). Arrangement of visual field on cat's cortex. Am. J. Physiol. 129, 477-478.

Thompson, J. M., Woolsey, C. N., and Talbot, S. A. (1950). Visual areas I and II of cerebral cortex of rabbit. *J. Neurophysio*. 12, 277-288.

Thompson, P.M., Lee, A.D., Dutton, R.A., Geaga, J.A., Hayashi, K.M., Eckert, M.A., Bellugi, U., Galaburda, A.M.;´, Korenberg, J.R., Mills, D.L., Toga, A.W. and Reiss, A.L. (2005). Abnormal Cortical Complexity and Thickness Profiles Mapped in Williams Syndrome. *The Journal of Neuroscience*, 25(16), 4146–4158.

Wade, N. and Swanston, M. (1991). Visual perception: an introduction. Routledge, London.

Wandell, B., Dumoulin, S., and Brewer, A. (2007). Visual Field Maps in Human Cortex. *Neuron*, 56, 366-383.